

172 ks Chandra Exposure of the LALA Boötes Field: X-ray Source Catalog

J. X. Wang¹, S. Malhotra², J. E. Rhoads², M. J. I. Brown³, A. Dey³, T. M. Heckman¹, B.
T. Jannuzi³, C. A. Norman^{1,2}, G. P. Tiede⁴, and P. Tozzi⁵

Received _____; accepted _____

¹Johns Hopkins University, Charles and 34th Street, Bloomberg center, Baltimore, MD 21218; jxw@pha.jhu.edu, heckman@pha.jhu.edu, norman@stsci.edu.

²Space Telescope Science Institute, 3700 San Martin Drive, Baltimore, MD 21218; san@stsci.edu, rhoads@stsci.edu.

³National Optical Astronomy Observatory, 950 North Cherry Avenue, Tucson, AZ 85719; mbrown@noao.edu, dey@noao.edu, jannuzi@noao.edu.

⁴Department of Physics and Astronomy, Bowling Green State University, Bowling Green, OH 43403; tiede@astro.ufl.edu

⁵Istituto Nazionale di Astrofisica (INAF) - Osservatorio Astronomico, Via G. Tiepolo 11, 34131 Trieste, Italy; tozzi@ts.astro.it

ABSTRACT

We present an analysis of a deep, 172 ks *Chandra* observation of the Large Area Lyman Alpha Survey (LALA) Boötes field, obtained with the Advanced CCD Imaging Spectrometer (ACIS-I) on the *Chandra* X-ray Observatory. This is one of the deepest *Chandra* images of the extragalactic sky; only the 2 Ms CDF-N and 1 Ms CDF-S are substantially deeper. In this paper we present the X-ray source catalog obtained from this image, along with an analysis of source counts, and optical identifications. The X-ray image is composed of two individual observations obtained in 2002, and reaches 0.5 – 2.0 and 2.0 – 10.0 keV flux limits of 1.5×10^{-16} and 1.0×10^{-15} ergs cm $^{-2}$ s $^{-1}$, respectively, for point sources near the aim point. A total of 168 X-ray sources were detected: 160 in the 0.5 – 7.0 keV band, 132 in the 0.5 – 2.0 keV band, and 111 in the 2.0 – 7.0 keV band. The X-ray source counts were derived and compared with those from other *Chandra* deep surveys; the hard X-ray source density of the LALA Boötes field is 33% higher than that of CDF-S at the flux level of 2.0×10^{-15} ergs cm $^{-2}$ s $^{-1}$, confirming the field-to-field variances of the hard band source counts reported by previous studies. The deep exposure resolves $\gtrsim 72\%$ of the 2.0 – 10.0 keV X-ray background.

Our primary optical data are *R*-band imaging from NOAO Deep Wide-Field Survey (NDWFS), with limiting magnitude of $R = 25.7$ (Vega, 3σ , 4" diameter aperture). We have found optical counterparts for 152 of the 168 *Chandra* sources (90%); 144 of these are detected on the *R*-band image, and 8 have optical counterparts in other bands (either B_W, V, I, z'). Among the *R*-band non-detected sources, not more than 11 of them can possibly be at $z > 5$, based on the hardness ratios of their X-ray emission and nondetections in bluer bands (B_W, V). The majority ($\sim 76\%$) of the X-ray sources are found to have $\log(f_X/f_R)$ within 0.0 ± 1 ,

which are believed to be AGNs. Most of the X-ray faint/optically bright sources ($\log(f_X/f_R) < -1.0$) are optically extended, which are low- z normal galaxies or low luminosity AGNs. There is also a population of sources which are X-ray *overluminous* for their optical magnitudes ($\log(f_X/f_R) > 1.0$), which are harder in X-ray and are probably obscured AGNs.

Subject headings: catalogs — galaxies: active — galaxies: high-redshift — X-rays: diffuse background — X-rays: galaxies

1. Introduction

A new era of X-ray astronomy has begun with the launch of the *Chandra X-Ray Observatory* on 1999 July 23, thanks to its very high sensitivity, broad energy range and high angular resolution (Weisskopf et al. 2002). The two deepest X-ray surveys ever conducted, 2 Ms *Chandra* Deep Field North (Brandt et al. 2003, Alexander et al. 2003) and 1 Ms *Chandra* Deep Field South (Giacconi et al. 2002; Rosati et al. 2001), were obtained using the Advanced CCD Imaging Spectrometer detector (ACIS; Garmire et al. 2003) on *Chandra X-Ray Observatory*. These two surveys are ~ 50 times more sensitive than the deepest pre-*Chandra* observations in the soft X-ray band (0.5 – 2.0 keV, e.g., Hasinger et al. 1998) and greater than 100 times more sensitive than those deepest pre-*Chandra* observations in the hard X-ray band (2.0 – 10.0 keV, e.g., Ueda et al. 1999; Fiore et al. 1999). With these surveys, the “diffuse” X-ray background discovered four decades ago (Giacconi et al. 1962) has been almost entirely resolved into discrete sources (i.e. $> 90\%$ in the soft band, and $\sim 80\%$ in the hard band).

Many other deep X-ray blank-sky surveys from *Chandra* (Stern et al. 2002a; Yang et al. 2003; Mushotzky et al. 2000; Manners et al. 2003) and XMM (Hasinger et al. 2001)

were also performed in the past few years. Along with multi-band observations of the detected X-ray sources, these deep surveys have brought us many interesting results and more important science issues to be addressed. These include the large scale structures from 2D (Yang et al. 2003) and 3D (Gilli et al. 2003; Barger et al. 2002) analyses, type 2 QSOs (Norman et al. 2002; Stern et al. 2002b), very high redshift X-ray selected Active Galactic Nuclei (AGN, e.g., Barger et al. 2003), and much more.

Here we present a new deep (172 ks) *Chandra* ACIS exposure, obtained originally for the follow-up of Ly α sources from the Large Area Lyman Alpha (LALA) survey’s Boötes field. The Large Area Lyman Alpha (LALA) Survey (Rhoads et al. 2000, 2003; Rhoads & Malhotra 2001, Malhotra & Rhoads 2002) was designed to search for Lyman α emitters at high redshifts through narrowband imaging. The survey comprises two primary fields, $36' \times 36'$ in size each, located in Boötes (at 14:25:57 +35:32 J2000.0) and in Cetus (at 02:05:20 -04:55 J2000.0). Both fields were chosen to be inside the large areas of the NOAO Deep Wide-Field Survey (NDWFS), which is a deep optical and IR ($B_W R I J H K$) imaging survey of 18 deg² of the sky with the primary goal of studying the evolution of large-scale structure from $z < 5$ (Jannuzi and Dey 1999; Brown et al. 2003; Jannuzi et al. 2004, in preparation). Five broadband optical images (B_W , R , I from NDWFS, and V , z' as part of LALA) and eight narrowband images are used to search for Lyman- α emitters at $z \sim 4.5$, 5.7, and 6.5 respectively. The X-ray image presented here was originally obtained to investigate the X-ray properties of the detected high redshift Ly α emitters. This study was presented by Malhotra et al. (2003), where we placed stringent upper limits on the typical X-ray flux of Ly α sources and conclude that AGN (obscured or otherwise) cannot constitute a dominant portion of the Ly α source population.

This *Chandra* exposure (172 ks) is among the deepest yet obtained by *Chandra* of the extragalactic sky; only the CDF-N and CDF-S are substantially deeper. In this

paper we present a full catalog of the detected X-ray sources, along with an analysis of the X-ray source counts, and the R -band magnitudes (or 3σ upper limits) for their optical counterparts. To study the nature of these sources, spectroscopic follow-up observations for these sources are under way.

The present paper is structured as follows: we present the X-ray observations and data reduction in Section 2, source detection and catalog in Section 3, LogN-LogS in section 4, and optical identifications in Section 5. Our conclusions and summary are presented in Section 6.

2. X-ray Observations and Data Reduction

An 178 kilo-second exposure, composed of two individual observations, was obtained using the Advanced CCD Imaging Spectrometer (ACIS) on the *Chandra X-ray Observatory* in the very faint (VFaint) mode. The first observation, with 120 ks exposure, was taken on 2002 April 16-17 (*Chandra* Obs ID 3130). The second observation, with 58 ks exposure, was taken on 2002 June 9 (Obs ID 3482). All four ACIS-I chips and ACIS-S2, ACIS-S3 chips were used, with the telescope aimpoint centered on the ACIS-I3 chip for each exposure. The aimpoint of Obs ID 3130 is 14:25:37.791 +35:36:00.20 (J2000.0⁶), and the aimpoint of Obs ID 3482 is 14:25:37.564 +35:35:44.32, 16'' away from that of Obs ID 3130. The Galactic column density N_H towards our field is $1.15 \times 10^{20} \text{ cm}^{-2}$ (Hartmann et al. 1996). Due to their large off-axis angle during the observations, the ACIS-S chips have worse spatial resolution and lower effective area relative to the ACIS-I chips. In this paper, data from any ACIS-S CCD were therefore ignored.

The data were reduced and analyzed using the *Chandra* Interactive Analysis of

⁶Coordinates throughout this paper are J2000.

Observations (CIAO) software (version 2.2.1, see <http://asc.harvard.edu/ciao>). The data were reprocessed to clean the ACIS particle background for very faint mode observations, and then filtered to include only the standard event grades 0,2,3,4,6⁷. All bad pixels and columns were also removed, not only from the photon events files, but also when calculating the effective exposure maps. The high background time intervals were manually removed by checking the total event rates. The total net exposure time is 172 ks (120 ks from Obs ID 3130, and 52 ks from Obs ID 3482). The offset between the astrometry of the two observations was obtained by registering the X-ray sources showing up in both exposures. The two event files were merged after correcting the small offset (0.3''), and the combined data have the same coordinate system as Obs ID 3130. We present the color composite X-ray image of the combined exposure in Fig. 1.

3. Source Detection and Catalog

Three images were extracted from the combined event file for source detection: a soft image (0.5 – 2.0 keV), a hard image (2.0 – 7.0 keV) and a total image (0.5 – 7.0 keV). The hard and total bands were cut at 7 keV since the effective area of *Chandra* decreases above this energy, and the instrumental background rises, giving a very inefficient detection of sky and source photons. The WAVDETECT program (Freeman et al. 2002), which is included with the CIAO software package, was run on the extracted images. A probability threshold of 1×10^{-7} (corresponding to 0.5 false sources expected per image), and wavelet scales of 1,2,4,8,16 pixels (1 pixel = 0.492'') were used. A total of 168 X-ray sources were detected: 160 in the total band (0.5 – 7.0 keV), 132 in the soft band (0.5 – 2.0 keV), and 111 in the hard band (2.0 – 7.0 keV). We present the catalog of the detected sources in

⁷see <http://asc.harvard.edu/proposer/POG/html/ACIS.html#sec:GRADES>

Table 1. Note that the number of total detected X-ray sources will be increased to 196 if we use a probability threshold of WAVDETECT (1×10^{-6}), however, considering the increased number of possible false detections (~ 5 expected per image), we prefer to publish a conservative catalog with fewer false detections. We also tried to search for X-ray sources with scales much larger than the PSF by running WAVDETECT with wavelet scales of 32,64,128 pixels on the images. However, we didn’t detect any new source beyond those in the catalog. Below we give explanations to the columns in Table 1.

Column(1)-(4): the source ID, IAU name, right ascension and declination respectively. The IAU name for the sources is CXOLALA1 JHHMMSS.s+DDMMSS. The positions were determined by WAVDETECT. Whenever possible, we use positions derived in the soft band, which has the best spatial resolution among the three bands. For sources which are not detected in the soft band, we use total band positions instead if available, and hard band positions were quoted for those sources detected only in the hard band.

Column(5): 3σ uncertainties of the centroid positions directly given by WAVDETECT.

Column(6)-(8): the net counts in the soft, hard and total bands. The counts were calculated using circular aperture photometry. For each source, we defined a source region which is a circle centered at the position given in column (3) and (4), with radius R_s set to the 95% encircled-energy radius of *Chandra* ACIS PSF at the source position. R_s varies in the range of $2''$ to $15''$ from the center to the edge of the field. Source photons were then extracted from the regions, and the local background was extracted from an annulus with outer radius of $2.4 \times R_s$ and inner radius of $1.2 \times R_s$, after masking out nearby sources. The aperture correction ($\times 1/0.95$) was applied to the source counts. The derived net counts and 1σ Poisson uncertainties (e.g., Gehrels 1986) are given for each source in each band.

Column(9): indication of source detection. We mark the source with “T”, “S” and “H”

for source detected in total, soft and hard band respectively. Multiple letters are used for sources detected in more than one band. For example, “TS” means detections in both the total band and the soft band, but non-detected in the hard band.

Column(10): hardness ratio defined as $HR = (H-S)/(H+S)$, where H and S are the vignetting-corrected net counts in the hard and soft band respectively. The hardness ratios vs 0.5 – 10.0 keV band X-ray fluxes for the detected X-ray sources are plotted in Fig. 2. Assuming a power-law spectrum with the Galactic HI column density ($1.15 \times 10^{20} \text{ cm}^{-2}$), the observed hardness ratio can be converted to the photon index Γ of the spectrum, which is also presented in the figure. As presented in earlier surveys, harder sources are seen at fainter fluxes, most of which are believed to be obscured AGNs.

Column(11)-(13): X-ray fluxes (Galactic absorption corrected) of three bands in the unit of $10^{-15} \text{ ergs cm}^{-2} \text{ s}^{-1}$. A power-law spectrum with the Galactic column density was assumed to calculate the conversion factors from net counts to X-ray fluxes. The photon index of the power-law was chosen at $\Gamma = 1.4$, which was also used in Giacconi et al. (2002) and Stern et al. (2002a). Three band net count rates were calculated by dividing the net counts in column 6-8 by the effective exposure time⁸ at each source position in each band, and then converted into X-ray fluxes of 0.5 – 10.0 keV, 0.5 – 2.0 keV, and 2.0 – 10.0 keV respectively. These settings make our results directly comparable with those from other surveys. The conversion factors used were $1.25 \times 10^{-11} \text{ ergs cm}^{-2} \text{ count}^{-1}$ from the 0.5 – 7.0 keV band observed count rates to the Galactic absorption corrected X-ray fluxes in the band 0.5 – 10.0 keV, $4.67 \times 10^{-12} \text{ ergs cm}^{-2} \text{ count}^{-1}$ from the 0.5 – 2.0 keV band count rates to the 0.5 – 2.0 keV band fluxes, and $2.96 \times 10^{-11} \text{ ergs cm}^{-2} \text{ count}^{-1}$ from the 2.0

⁸The effective exposure time was calculated through multiplying 172 ks by the ratio of the exposure map at the aim point to the value of the exposure map averaged within the extraction region for each source. Such a correction was done in each band separately.

– 7.0 keV band count rates to the 2.0 – 10.0 keV band fluxes. Note the total band (0.5 – 10.0 keV) flux is not equal to the sum of the soft and hard band fluxes if the actual photon index differs from 1.4. To calculate the fluxes assuming a power-law spectrum with different photon index Γ , the conversion factors $F_\Gamma/F_{1.4}$ for different bands are needed (Fig. 3). We can see from the figure that the soft band (0.5 – 2.0 keV) flux is not sensitive to the photon index Γ , while the hard (2.0 – 10.0 keV) and total (0.5 – 10.0 keV) band fluxes correlate with it strongly. One thus has to be careful while using these fluxes.

Column(14)-(16): The offsets of the detected optical counterparts from the X-ray source positions ($\Delta\alpha = \text{RA}_R - \text{RA}_X$, $\Delta\delta = \text{Dec}_R - \text{Dec}_X$), and the R -band AUTO magnitudes (Kron-like elliptical aperture magnitudes, Bertin & Arnouts 1996) with 1σ uncertainties⁹. For sources which are not detected in R -band, 3σ upper limits of the magnitudes are given when available. See section 5 for details.

Column(17): The FWHM (full-width half-maximum) of the optical counterparts in NDWFS R -band image (see section 5).

4. X-ray source counts

In order to calculate the cumulative source counts, $N(>S)$, one need count the number of sources with fluxes $>S$, and also compute the summed sky in the field where these sources can be detected (the sky coverage). In Fig. 4, we present the soft and hard band net counts vs off-axis angle for faint sources (with net counts < 50). Detected and non-detected sources (detected in other bands but having net counts from X-ray photometry) are displayed with different symbols. It's clear from the figure that the X-ray sources with larger off-axis angles

⁹The uncertainties of the magnitudes are direct output from SExtractor, without including the uncertainty of the R -band zeropoint.

need more net counts to be detected because of the larger PSF size. This indicates that the detection limits of net counts vary with the PSF sizes. Two dashed lines (net counts = $A + B \times \text{PSF}^2$ respectively) are added to Fig. 4, with the parameters A and B chosen for both bands by visual inspection to exclude all non-detected sources and include maximum number of detected sources. We can see that although some detected sources are located below the threshold dashed lines, they are mixed up with these non-detected sources, i.e., the detection is incomplete below the lines, and the sky coverage for these sources is thus not available. In this paper, we use only these sources with net counts $C > A + B \times \text{PSF}^2$ to calculate LogN-LogS¹⁰. Using the above cutoffs, the sky coverages are derived and presented in Fig. 5. The derived LogN-LogS for both soft and hard band are presented in Fig. 6. A maximum-likelihood power-law was used to fit the slope of the LogN-LogS in each band. For the 0.5 – 2.0 keV band we find

$$N(> S) = 340 \left(\frac{S}{2 \times 10^{-15} \text{ ergs cm}^{-2} \text{ s}^{-1}} \right)^{-0.78} \quad (1)$$

And for the 2.0 – 10.0 keV band, we find:

$$N(> S) = 1790 \left(\frac{S}{2 \times 10^{-15} \text{ ergs cm}^{-2} \text{ s}^{-1}} \right)^{-1.16} \quad (2)$$

The above procedures of calculating LogN-LogS were also run on the 1 Ms CDF-N data (Brandt et al. 2001), 1 Ms CDF-S data (Rosati et al. 2002), and 184.7 ks Lynx data (Stern et al. 2002a). The independently derived LogN-LogS from the above three fields match the published ones to within 1σ , and are plotted in Fig. 6 for comparison. The source densities ($N>S$) and 1σ uncertainties at the faint end ($2.0 \times 10^{-16} \text{ ergs cm}^{-2} \text{ s}^{-1}$ in 0.5 – 2.0 keV band, and $2.0 \times 10^{-15} \text{ ergs cm}^{-2} \text{ s}^{-1}$ in the 2.0 – 10.0 keV band) are plotted in the inserts. In the soft band, there is no significant difference among the source counts from the four deep surveys. In the hard band, obvious fluctuations of the source counts are seen at the

¹⁰ $A = 5.3, 8.2$ and $B = 0.026, 0.053$ for the soft and hard band respectively.

faint end: LALA Boötes field has the highest source density at 2.0×10^{-15} ergs cm⁻² s⁻¹ which is 33% higher than that of CDF-S, while CDF-N is 23% higher than CDF-S and Lynx field is 14% lower. Note that similar field-to-field variances of the hard band source counts have been reported previously (see Tozzi 2001a, Cowie et al. 2002). This is believed to be due to the clustering of the X-ray sources. The non-detection of field-to-field variance in the soft band is also consistent with the results from previous studies (Yang et al. 2003; Tozzi et al. 2001a), indicating that the soft X-ray sources are less correlated than the hard X-ray sources.

What fraction of the hard X-ray background is resolved by our deep 172 ks *Chandra* imaging? In the range of 1.7-100 × 10⁻¹⁵ ergs cm⁻² s⁻¹, the integrated hard X-ray flux density in the 2.0 – 10.0 keV band is 1.2 × 10⁻¹¹ ergs cm⁻² s⁻¹ deg⁻². Note for sources bright than 10⁻¹³ ergs cm⁻² s⁻¹, the integrated hard X-ray flux density from our survey is 0.4 × 10⁻¹¹ ergs cm⁻² s⁻¹ deg⁻², consistent with the value derived by della Ceca et al. (1999) from a wider area ASCA survey. The total integrated hard X-ray flux density we obtained is 1.6 × 10⁻¹¹ ergs cm⁻² s⁻¹ deg⁻², down to 1.7 × 10⁻¹⁵ ergs cm⁻² s⁻¹ in 2.0 – 10.0 keV band. This is equal to the High Energy Astronomy Observatory 1 (HEAO 1) value (Marshall et al. 1980), but 10%-30% lower than the more recent determinations from ASCA and *BeppoSAX* (e.g., Ueda et al. 1999; Vecchi et al. 1999). We conclude that our 172 *Chandra* deep imaging resolves $\gtrsim 70\%$ of the 2.0 – 10.0 keV X-ray background, and the main uncertainty comes from the value of total X-ray background itself.

5. Optical Identifications

5.1. Optical Images

Our deep Chandra pointing is within the NDWFS Boötes subfield NDWFS J1426+3531 (which is $35' \times 35'$ in size) centered at RA 14:26:00.8, DEC +35:31:32.0 (J2000). Five broadband optical images (B_W , V , R , I , and z') are available to search for the optical counterparts of the X-ray sources. Three of these (B_W , R , and I)¹¹ are from the NOAO Deep Wide Field Survey (NDWFS; Jannuzi & Dey 1999), while the remaining two (V and z') were obtained as part of LALA. The limiting Kron-Cousins system magnitudes (3σ , $4''$ diameter aperture) of the NDWFS images are $B_W < 26.5$, $R < 25.7$, and $I < 25.0$. The corresponding limits in the LALA broadband data are $V < 25.9$ and $z' < 24.6$ (where the z' limit is on the AB system). Our primary optical image for identifications in this paper is the R -band image from NDWFS, which is substantially deeper than the others. All the optical images were obtained using the Kitt Peak National Observatory Mayall 4m telescope and the Mosaic-1 camera (Muller et al. 1998; Jannuzi et al. 2004, in preparation). These images were produced following the procedures described in version 7.01 of "The NOAO Deep Wide-Field Survey MOSAIC Data Reductions"¹². A general description of the software used is provided by Valdes (2002) and the complete details of the NDWFS data reduction will be provided by Jannuzi et al. (2004).

¹¹The B_W and I band images are available from the NOAO Science Archive (<http://www.archive.noao.edu/ndwfs/>). The R -band image, which is deeper than the currently released version, will be available from the NOAO Science Archive within 12 months.

¹²<http://www.noao.edu/noao/noadeep/ReductionOpt/frames.html>.

5.2. Optical Counterparts

SExtractor package (Bertin & Arnouts 1996) V2.1.0 was run on the NDWFS deep R -band image to generate the R -band source catalog. The registration of the X-ray to optical coordinates was done by cross-correlating the X-ray and the above R -band catalogs (e.g., see Giacconi et al. 2002, Stern et al. 2002a). Average shifts in ($RA_R - RA_X$, $Dec_R - Dec_X$) of (0.1", -0.2") were found from the NDWFS R -band to X-ray imaging, but no obvious rotation or plate-scale effects were discovered. After correcting the average shifts, we matched the optical and X-ray source catalogs using a 1.5" radius aperture for host identifications, which was generally used by other *Chandra* surveys (Giacconi et al. 2002, Stern et al. 2002a). The 3σ X-ray positional uncertainties in Table 1 are used if larger than 1.5".

Optical counterparts for 144 of the 168 X-ray sources were detected in the R -band image down to 3σ . One of them (No. 122) has multiple possible optical counterparts. Calculations show that the possibility of having one optical source down to 3σ in a 1.5" circle by chance is 10%. This means that at least 90% of the optical counterparts we found should correspond to the X-ray sources, and at worst we might have ~ 14 false matches.

We present the offsets from the X-ray source positions ($\Delta\alpha = RA_R - RA_X$, $\Delta\delta = Dec_R - Dec_X$), the derived R -band AUTO magnitudes (Kron-like elliptical aperture magnitudes, Bertin & Arnouts 1996) for all optical counterparts in Table 1, and the optical cutouts in Fig. 7. IRAF package "radprof" was used to measure the radial profiles of these counterparts in NDWFS R image, and we present the measured FWHM (full-width half-maximum) in Table 1. These sources which have FWHM larger than the average seeing of the NDWFS R image (FWHM = 1.16") were examined visually. We conclude that it is safe to consider all the bright sources ($R < 23$) with FWHM $\geq 1.3''$ as optically resolved. The only exception is source No. 144, which is too close to another bright source, thus we

can not tell if it is resolved or not. The total number of optically resolved sources is 15.

The search for optical counterparts was extended to B_W , I , V and z' band for the 24 X-ray sources without R -band optical counterparts, which brought us optical counterparts for 8 more X-ray sources. The positions of these counterparts are also given in Table 1 (by listing RA - RA_X, Dec - Dec_X). The limiting magnitude of the R -band image was given as upper limits for 22 of the X-ray sources. Note source No. 37 and 160 are overlapped by bleeding trails in the NDWFS R image, and the upper limits of their R -band magnitudes are not available.

The FIRST survey (Faint Images of the Radio Sky at Twenty-cm, Becker, White, & Helfand 1995) detection limit in our field is 0.96 mJy/beam. Radio counterparts for 4 of our X-ray sources were found, which are source No. 1, 66, 91 and 141, with integrated flux density (mJy) of 6.02, 1.24, 2.17 and 8.30 respectively. The first 3 of the 4 radio sources are resolved R<21 red galaxies, which are some of the brightest optical counterparts to X-ray sources in our catalog. The remaining source is an R-band non-detection more than 10" from any R<21 galaxies and is presumably at $z > 1$.

5.3. X-ray-to-optical flux ratio

In Fig. 8 we plot the X-ray-to-optical flux ratio of our X-ray sources (in soft and hard band respectively), and in Fig. 9 we plot the $\log(f_X/f_R)$ in the hard band vs the hardness ratio of X-ray emission. For the 22 X-ray sources without R -band counterparts detected, the lower limits of $\log(f_X/f_R)$ were plotted, which shows a consistent distribution with that of the optically faint ($R > 24$) sources. From the figures we can see that the majority ($\sim 76\%$) of the X-ray sources fall within $\log(f_{2-10keV}/f_R) = 0.0 \pm 1$, which is typical of AGNs.

There is a significant population ($\sim 10\%$) of X-ray faint/optically bright sources

($\log(f_{2-10\text{keV}}/f_R) < -1.0$), most of which are extended in the R band optical image and X-ray soft (see Fig. 9). These sources should be nearby, bright normal galaxies (see Tozzi et al. 2001b; Barger et al. 2001; Hornschemeier et al. 2001). Other optically extended sources falling within $\log(f_{2-10\text{keV}}/f_R) = 0.0 \pm 1$ or X-ray hard are most likely to be low redshift Seyfert galaxies, or low luminosity AGNs.

In addition, we also have a population of sources which are X-ray *overluminous* for their optical magnitudes ($\log(f_{2-10\text{keV}}/f_R) > 1.0$), especially in the hard band, including most of the 22 R -band nondetected X-ray sources. We plot in Fig. 10 the histogram distribution of the hardness ratios of the optically faint X-ray bright sources ($\log(f_{2-10\text{keV}}/f_R) > 1.0$), comparing with these sources with lower X-ray-to-optical flux ratio ($1.0 > \log(f_{2-10\text{keV}}/f_R) > 0.0$). The optically faint X-ray bright sources are obviously harder in X-ray, suggesting that most of them are obscured AGNs, for which high column density absorption shields both the optical and the soft X-ray emission.

5.4. R -band nondetections

There are 22 X-ray sources which are not detected in the R -band down to $R = 25.7$; 5 of them are detected in redder bands (I, z'); and 3 of them in bluer bands (B_W, V); 14 X-ray sources have no optical counterparts found in any band, which corresponds to a sky surface density of 145 deg^{-2} . The integrated hard X-ray (2.0 – 10.0 keV) flux density from these 22 sources is $0.14 \times 10^{-11} \text{ ergs cm}^{-2} \text{ s}^{-1} \text{ deg}^{-2}$, down to a flux limit of $1.7 \times 10^{-15} \text{ ergs cm}^{-2} \text{ s}^{-1}$. This contributes 6~9% of the total 2.0 – 10.0 keV band X-ray background.

The 19 R -band nondetected sources, which are not detected in bluer bands (B_W, V), are possible candidates for $z > 5$ quasars, because of the absorption from the Lyman transitions of hydrogen along our line of sight. However, our calculations indicate that even

for a Compton thick AGN (with intrinsic photon power-law index $\Gamma = 2.0$ and absorption column density $N_H = 10^{24} \text{ cm}^{-2}$), the hardness ratio HR is expected to be < 0 at $z > 5$. Thus 8 of them with harder X-ray spectra ($\text{HR} > 0$) can not be at $z > 5$. In Fig. 9, we also marked the 5 X-ray sources without R -band counterparts, but showing up in redder bands (I, z'). Preliminary results from photometric redshift analyses show that the two softest ones of the 5 are at photo- $z \sim 4.3$, and the other 3 which have harder X-ray spectra at photo- $z \sim 1-2$. This agrees well with the above argument that high redshift objects should be soft in X-ray. Excluding these sources with $\text{HR} > 0$, there are 11 R -band nondetections left, which can be possibly at $z > 5$.

Assuming a constant AGN density up to $z = 10$, Gilli, Salvati & Hasinger (2001) predicted a $z > 5$ AGN density of 500 deg^{-2} for a limiting flux of $2.3 \times 10^{-15} \text{ ergs cm}^{-2} \text{ s}^{-1}$ in the 0.5 – 2.0 keV band. This model predicts ~ 50 $z > 5$ sources in our field, which is clearly too high. Assuming the AGN density above $z = 2.7$ decreases by a factor of 2.7 per unit redshift as found for optical quasars (Schmidt, Schneider, & Gunn 1995), Gilli et al. predicted a much lower source density of $z > 5$ AGNs (25 deg^{-2}) for the same limiting flux. It corresponds to ~ 2 $z > 5$ objects in our field, which is very plausible with the current data, considering that those 11 sources are unlikely to be all at $z > 5$. Actually, several optically faint *Chandra* sources from other surveys have already been confirmed to be at $z < 5$ by spectroscopic observations (e.g., see Alexander et al. 2001).

6. Conclusions

We present a deep, 172 ks *Chandra* ACIS exposure of the LALA Boötes field. This paper describes the details of the observations, data reduction, source detection, LogN-LogS analysis, and presents the X-ray source catalog along with R -band magnitudes of their optical counterparts. A total of 168 X-ray sources were detected, 160 in the total band

(0.5 – 7.0 keV), 132 in the soft band (0.5 – 2.0 keV), and 111 in the hard band (2.0 – 7.0 keV). Near the aim point, the detection is down to a flux limit of 1.5×10^{-16} ergs cm^{-2} s^{-1} in soft (0.5 – 2.0 keV) band, and 1.0×10^{-15} ergs cm^{-2} s^{-1} in hard (2.0 – 10.0 keV) band. LogN-LogS was compared with those from other deep surveys, and we find obvious field-to-field fluctuations of the hard band source counts. These fluctuations are believed to be due to the large scale clustering of the detected X-ray sources. Calculations show that our deep imaging resolves $\gtrsim 70\%$ of the X-ray background in 2.0 – 10.0 keV band. Optical counterparts for 90% of the X-ray sources were found from deep optical images. Among the *R*-band non-detected sources, 11 of them can be possibly at $z > 5$, based on the hardness ratios of their X-ray emission and the fact that they are not detected in bluer bands (B_W, V). Spectroscopic follow-up observations of these counterparts are being undertaken and will be present in future paper.

This work was supported by the CXC grant GO2-3152X and the National Optical Astronomy Observatory which is operated by the Association of Universities for Research in Astronomy (AURA), Inc. under a cooperative agreement with the National Science Foundation. We would like to thank the NDWFS team, and in particular Melissa Miller (NOAO), who assisted in the reduction of the *R*-band image used extensively in this paper. We would like to thank N. Brandt for providing the CDF-N LogN - LogS. We also thank the referee for a prompt and helpful report.

REFERENCES

- Alexander, D. M., Brandt, W. N., Hornschemeier, A. E., Garmire, G. P., Schneider, D. P.,
Bauer, F. E., & Griffiths, R. E 2001, AJ, 122, 2156
- Alexander, D. M., et al. 2003, AJ, in press, astro-ph/0304392
- Barger, A. J., Cowie, L. L., Mushotzky, R. F., & Richards, E. A. 2001, AJ, 121, 662
- Barger, A. J., Cowie, L. L., Brandt, W. N., Capak, P., Garmire, G. P., Hornschemeier, A.
E., Steffen, A. T., & Wehner, E. H. 2002, AJ, 124, 1839
- Barger, A. J., Cowie, L. L., Capak, P., Alexander, D. M., Bauer, F. E., Brandt, W. N.,
Garmire, G. P., & Hornschemeier, A. E. 2003, ApJ, 584, 61
- Becker, R. H., White, R. L., & Helfand, D. J. 1995, ApJ, 450, 559
- Bertin, E. and Arnouts, S. 1996, A&AS 117,393
- Brandt, W. N., et al. 2001, 122, 2810
- Brandt, W. N., et al. 2003, HEAD, 35, 3601B
- Brown, M, Dey, A, Jannuzi, B. T., Lauer, T. R., Tiede, G. P., & Mikles, V. J. 2003, ApJ,
in press, astro-ph0306128
- Cowie, L. L., Garmire, G. P., Bautz, M. W., Barger, A. J., Brandt, W. N., & Hornschemeier,
A. E. 2002, ApJ, 566, L5
- della Ceca, R., Castelli, G., Braitto, V., Cagnoni, I., & Maccacaro, T. 1999, ApJ, 524, 674
- Fiore, F., La Franca, F., Giommi, P., Elvis, M., Matt, G., Comastri, A., Molendi, S., &
Gioia, I. 1999, MNRAS, 306, L55
- Freeman, P.E., Kashyap, V., Rosner, R., & Lamb, D. Q. 2002, ApJS, 138, 185
- Garmire, G. P., Bautz, M. W., Ford, P. G., Nousek, J. A., & Ricker, G. R. 2003, Proc.
SPIE, 4851, 28

- Gehrels, N. 1986, *ApJ*, 303, 336
- Giacconi, R., Gurksy, H., Paolini, F.R., & Rossi, B.B. 1962, *Phys. Rev. Lett.*, 9, 439
- Giacconi, R., et al. 2002, *ApJS*, 139, 369
- Gilli, R., Salvati, M., & Hasinger, G. 2001, *A&A*, 366, 407
- Gilli, R. et al. 2003, *ApJ Letter* accepted
- Hornschemeier, A. E. et al. 2001, *ApJ*, 554, 742
- Hartmann, D, Kalberla, P. M. W., Burton, W. B., & Mebold, U. 1999, *A&AS*, 119, 115
- Hasinger, G., Burg, R., Giacconi, R., Schmidt, M., Trumper, J., & Zamorani, G. 1998, *A&A*, 329, 482
- Hasinger, G. et al. 2001, *A&A*, 365, L45
- Jannuzi, B. T., & Dey, A. 1999, in *ASP Conf. Ser.* 191, *Photometric redshifts and High-Redshift Galaxies*, ed. R. J. Weymann, L. J. Storrie-Lombardi, M. Sawicki, & R. J. Brunner (San Francisco: ASP), 111
- Malhotra, S. & Rhoads, J. E. 2002, *ApJ*, 565, L71
- Malhotra, S., Wang, J. X., Rhoads, J. E., Heckman, T. M., & Norman, C. A. 2003, *ApJ*, 585, L25
- Manners, J. C., et al. 2003, *MNRAS*, 343, 293
- Muller, G. P., Reed, R., Armandroff, T., Boroson, T. A., & Jacoby, G. H. 1998, *Proc. SPIE*, 3355, 577
- Mushotzky, R. F., Cowie, L. L., Barger, A. J., & Arnaud, K. A. 2000, *Nature*, 404, 459
- Norman, C, et al. 2002, *ApJ*, 571, 218
- Rhoads, J. E., Malhotra, S., Dey, A., Stern, D., Spinrad, H., & Jannuzi, B. T. 2000, *ApJ*, 545, L85

- Rhoads, J. E., & Malhotra, S. 2001, *ApJ*, 563, L5
- Rhoads, J. E., et al. 2003, *AJ*, 125, 1006
- Rosati, P., et al. 2002, *ApJ*, 566, 667
- Schmidt, M., Schneider, D. P., & Gunn, J. E. 1995, *AJ*, 110, 68
- Stern, D., et al. 2002a, *ApJS*, 123, 2223
- Stern, D., et al. 2002b, *ApJ*, 568, 71
- Tozzi, P. 2001a, in *Proc. Marseille 2001 Conf. Where's the Matter?* eds. L. Tresse & M. Treyer, astro-ph/0111036
- Tozzi, P. et al. 2001b, *ApJ*, 562, 42
- Ueda, Y., et al. 1999, *ApJ*, 518, 656
- Valdes, F. G. 2002, in *Automated Data Analysis in Astronomy*, eds. Ranjan Gupta, Harinder P. Singh, and Coryn A. L. Bailer-Jones, (New Delhi: Narosa Publishing House), 309.
- Vecchi, A., Molendi, S., Guainazzi, M., Fiore, F., & Parmar, A. N. 1999, *A&A*, 349, L73
- Weisskopf, M. C., Brinkman, B., Canizares, C., Garmire, G., Murray, S., & Van Speybroeck, L. P. 2002, *PASP*, 114, 1
- Yang, Y., Mushotzky, R. F., Barger, A. J., Cowie, L. L., Sanders, D. B., & Steffen, A. T. 2003, *ApJ*, 585, L85

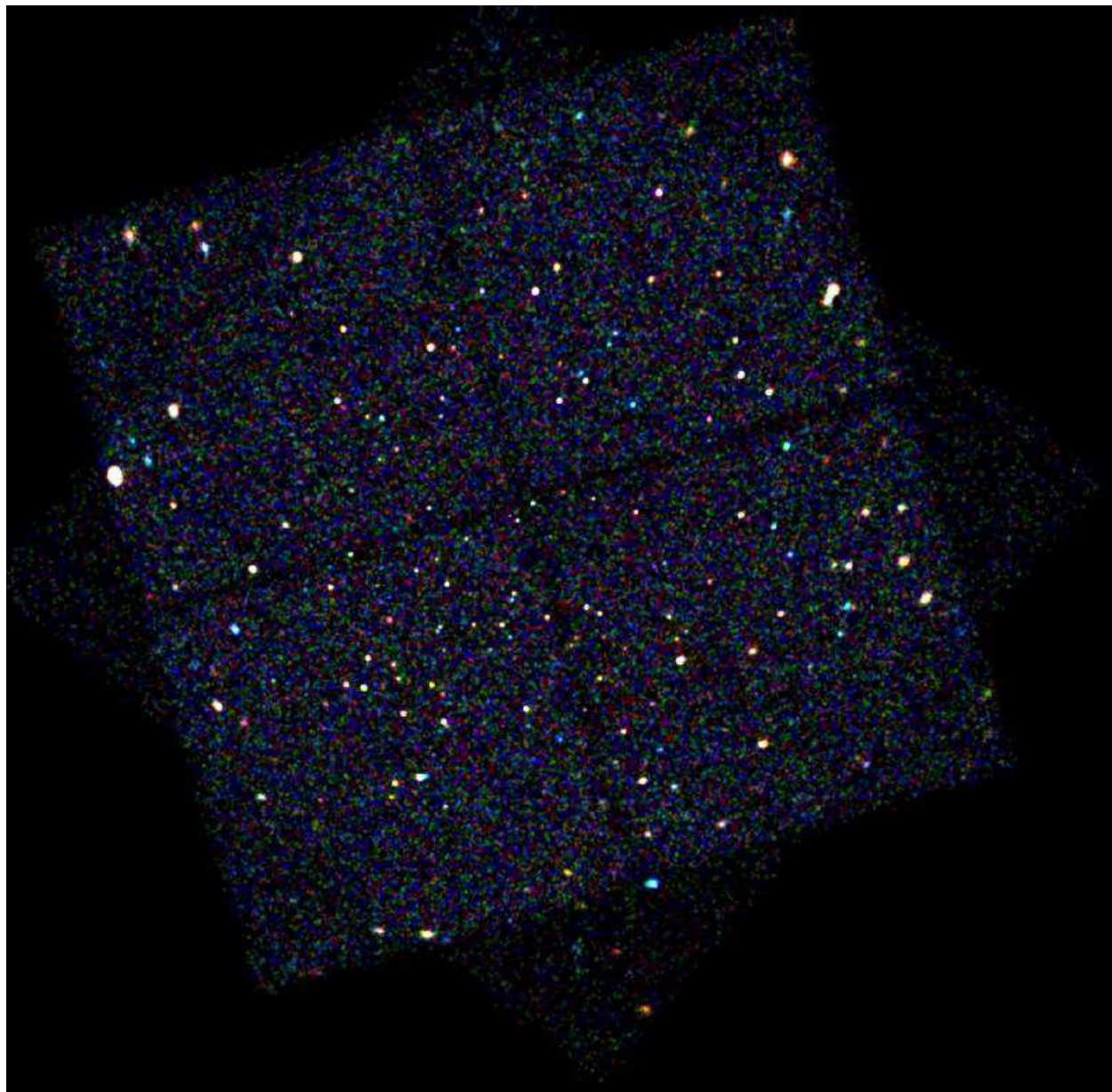


Fig. 1.— False-color X-ray image ($25' \times 25'$) of the LALA Boötes Field, composed from 172 ks *Chandra* exposure. North is to the top, and east is to the left. The image was obtained combining three energy bands: 0.3 – 1.0 keV, 1.0 – 2.0 keV, 2.0 – 7.0 keV (red, green and blue respectively). The color intensity is derived directly from the counts and has not been corrected for vignetting.

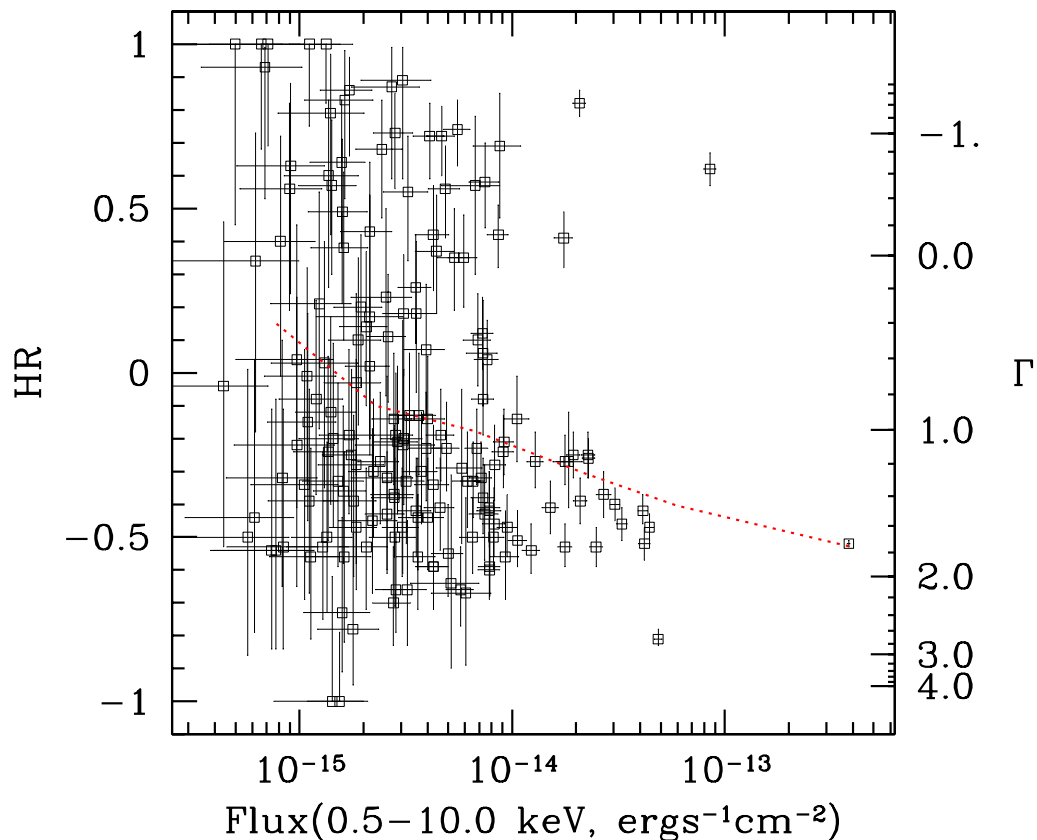


Fig. 2.— Hardness ratios $HR = (H - S)/(H + S)$ (left ordinate axis) of X-ray sources vs their full band (0.5 – 10.0 keV) X-ray fluxes. The photon indices Γ of the power-law spectra which could reproduce the observed hardness ratios are given along the right ordinate (see text for details). The dotted line connects the averaged hardness ratios for detected sources within different flux bins.

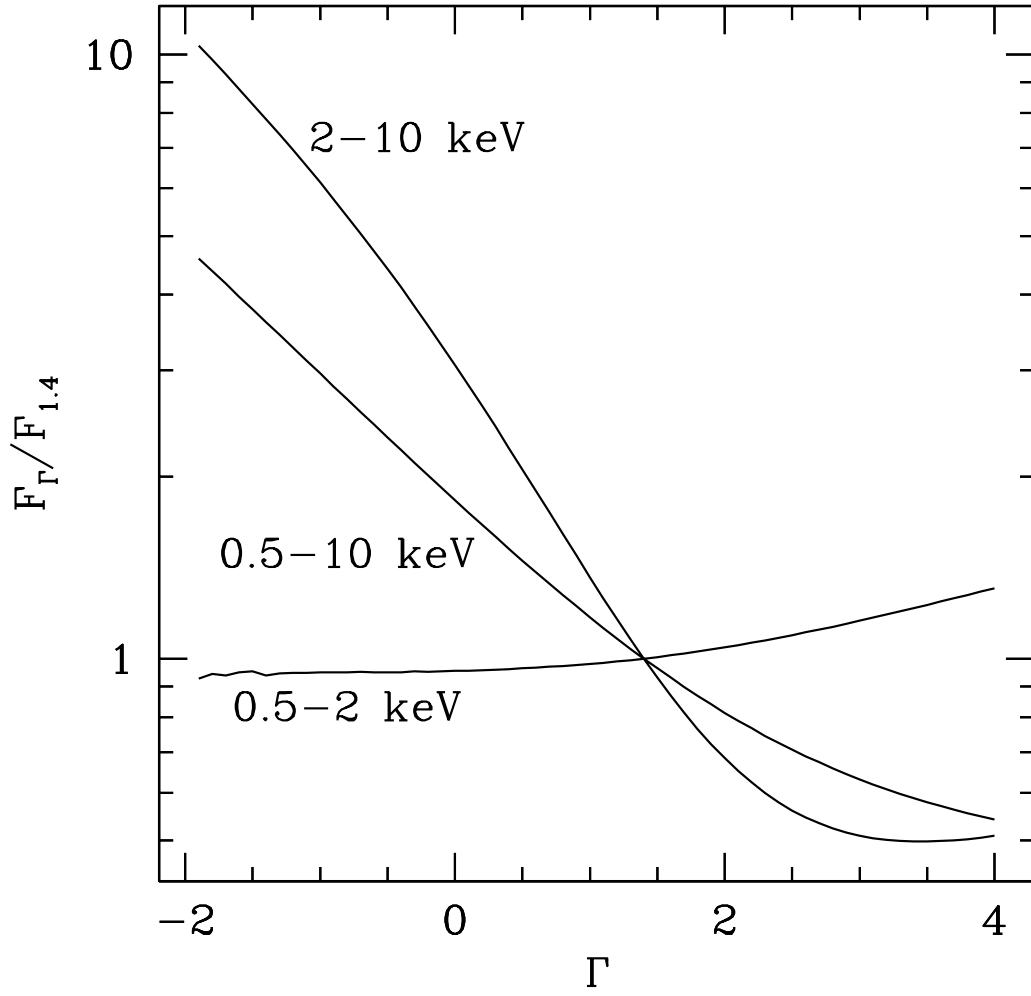


Fig. 3.— Conversion factors to calculate three band fluxes assuming a power-law spectrum with photon index different from $\Gamma = 1.4$.

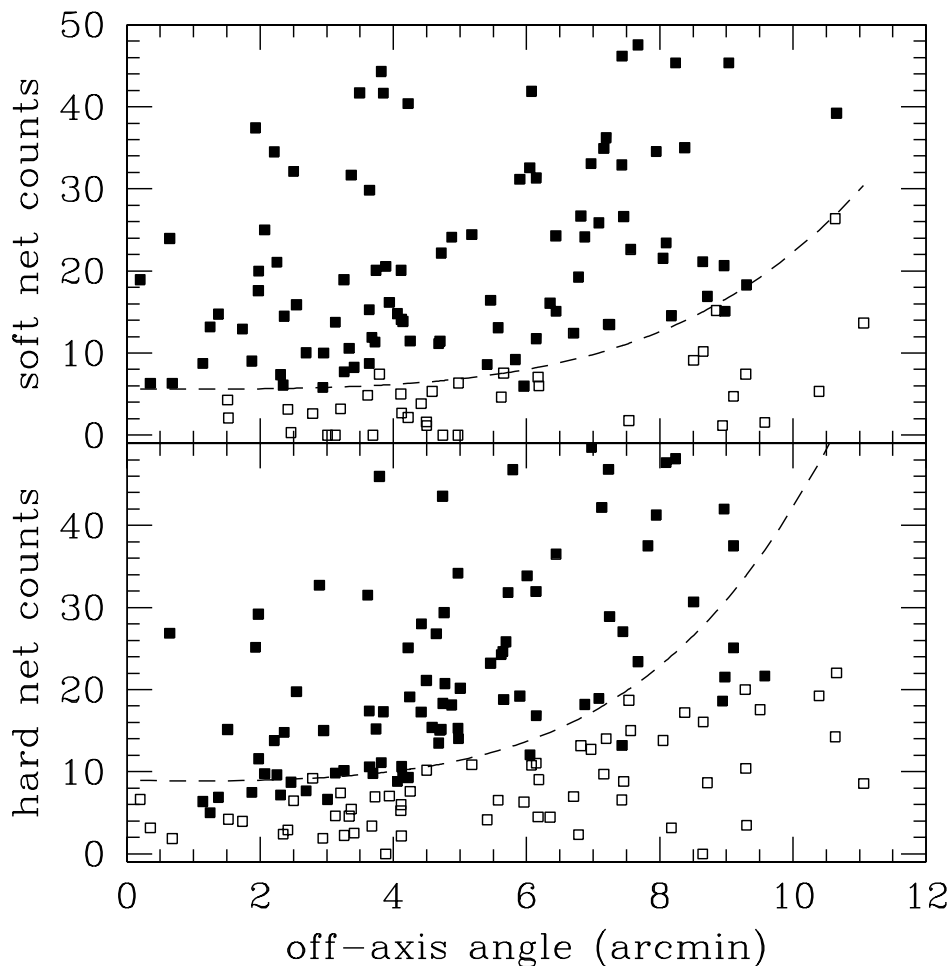


Fig. 4.— Soft (0.5 – 2.0 keV) and hard (2.0 – 7.0 keV) band net counts vs off-axis angle. The two dashed lines are the threshold we chose to build complete samples for LogN-LogS calculation. The net counts are derived from X-ray photometry. Thus for each source we can give net count for each band, whether it is detected in the band or not. In the upper panel, the filled squares are sources detected in the soft band, and open ones are those not detected in the soft band. In the lower panel, the filled squares are sources detected in the hard band, and open ones are those not detected in the hard band.

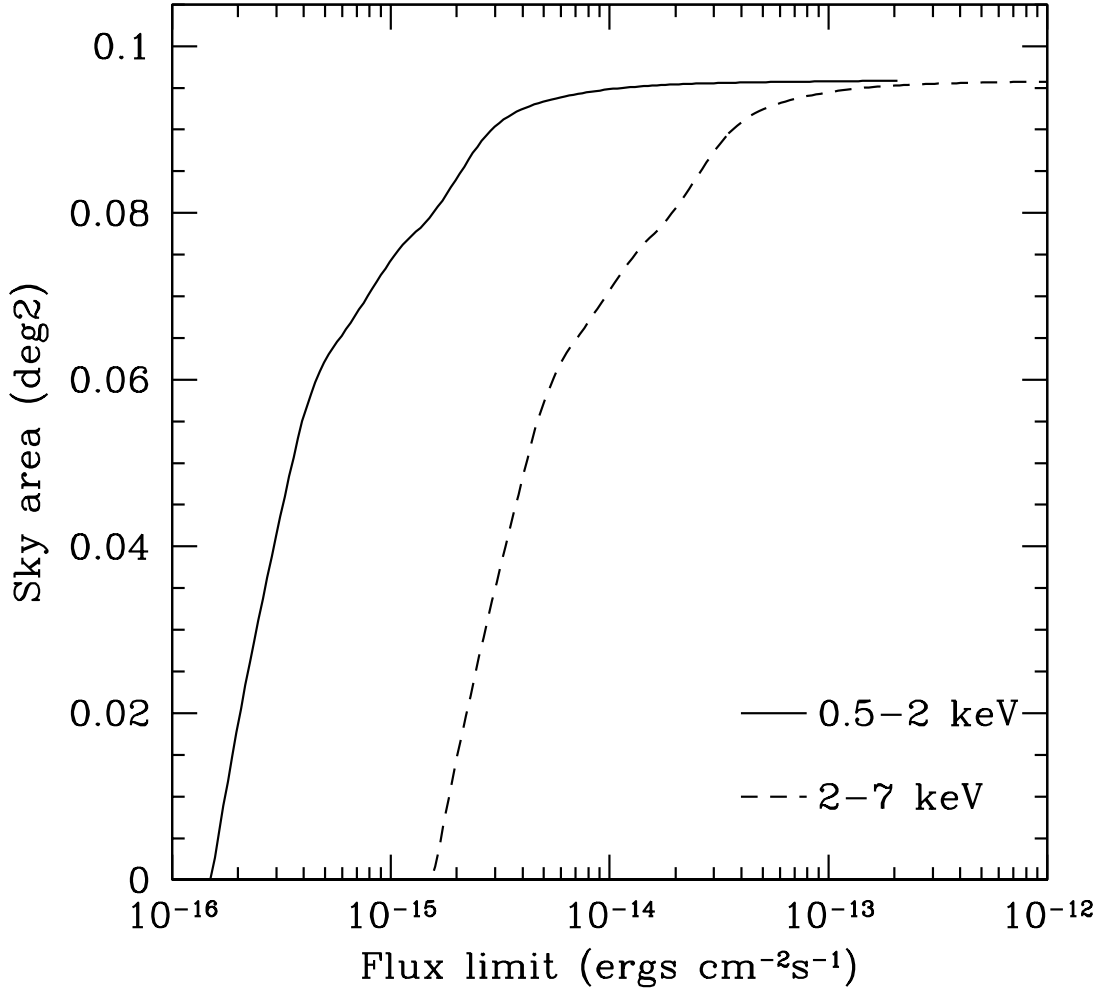


Fig. 5.— Sky coverage in soft (0.5 – 2.0 keV) and hard (2.0 – 7.0 keV) bands, as a function of flux limit.

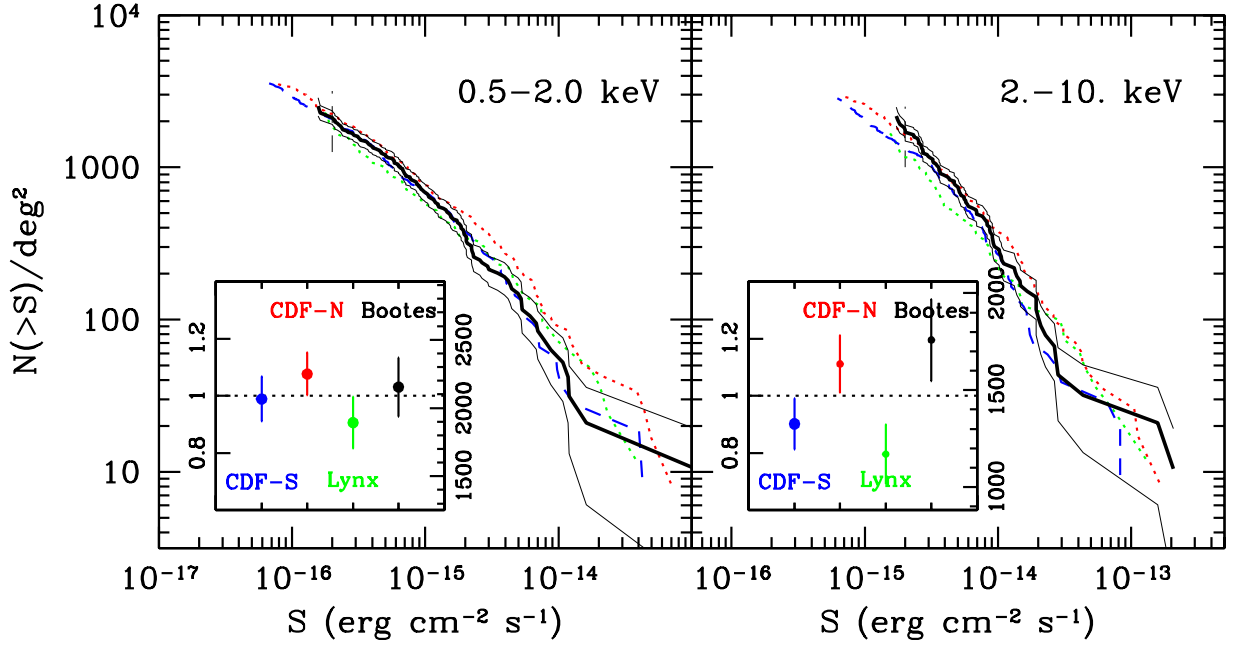


Fig. 6.— LogN-LogS in the soft (0.5 – 2.0 keV) and hard (2.0 – 10.0 keV) bands from 172ks *Chandra* observations of LALA Boötes field. Data are plotted as thick solid lines with two additional thin solid lines enclosing 1σ Poisson uncertainties. LogN-LogS from CDF-N, CDF-S and Lynx field are also plotted (see text for details). The inserts show the X-ray source densities and 1σ uncertainties from the four fields at the faint end of our 172 ks *Chandra* exposure (2.0×10^{-16} ergs cm^{-2} s^{-1} in 0.5 – 2.0 keV band, and 2.0×10^{-15} ergs cm^{-2} s^{-1} in the 2.0 – 10.0 keV band). The dashed lines in the inserts are the average source densities from the four fields, and the scales of the inserts are 0.6 to 1.4 times the average values.

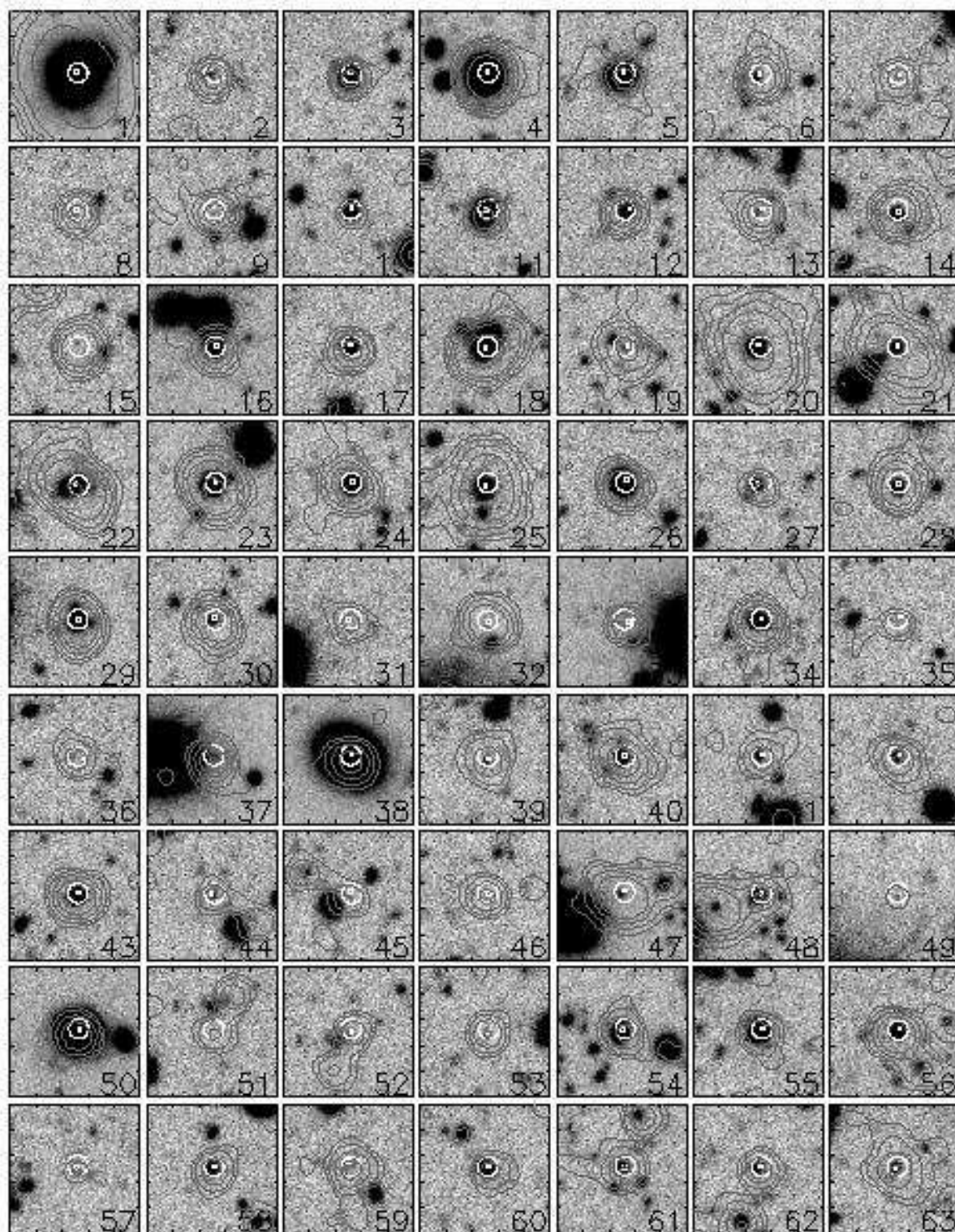


Fig. 7.—

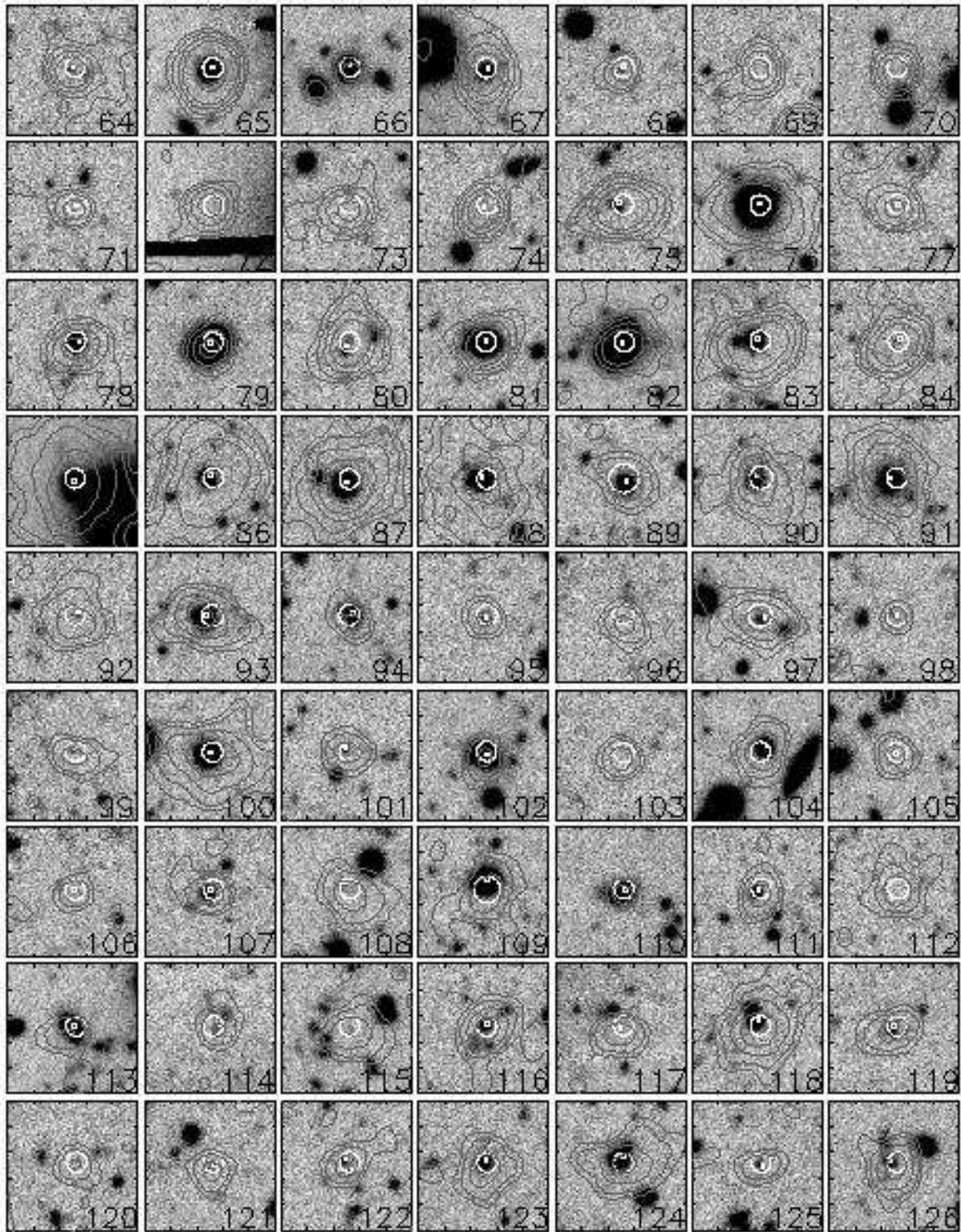


Fig. 7.—

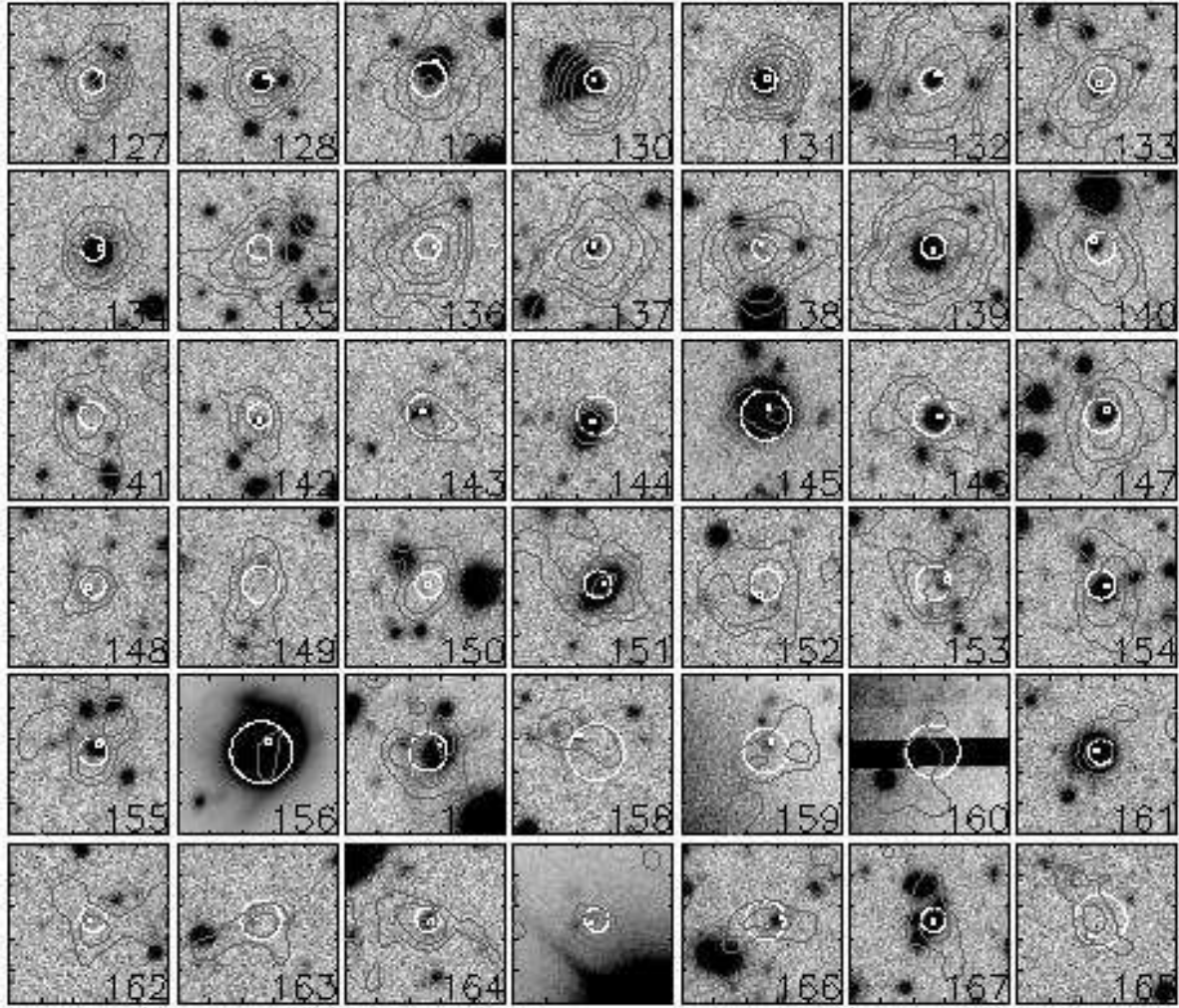


Fig. 7.— Optical cutouts ($20'' \times 20''$) for the 168 X-ray sources, overlapped by black X-ray isointensity contours (at 3,5,10,20 and 100σ above the local background). The small white box indicates an optical counterpart candidate, and the circle in the center indicates the radius used to search counterparts. North is to the top, and east is to the left.

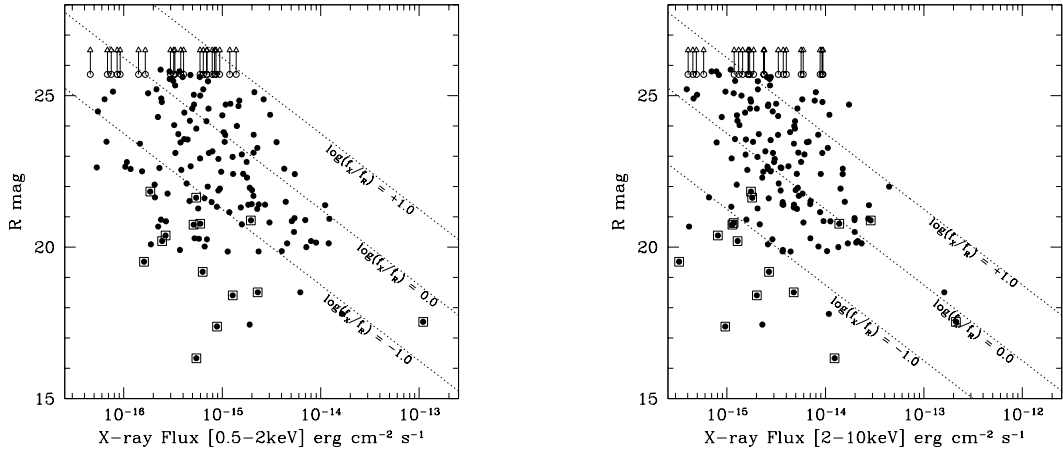


Fig. 8.— Optical R -band magnitudes of the X-ray detected sources vs their soft (0.5 – 2.0 keV) and hard (2 – 10 keV) X-ray fluxes. 3σ upper limits are plotted for sources without R -band counterparts. Dotted lines show location of constant X-ray-to-optical flux ratio $\log(f_X/f_R)$ of +1, 0, and -1. Dots enclosed by squares are optically extended sources.

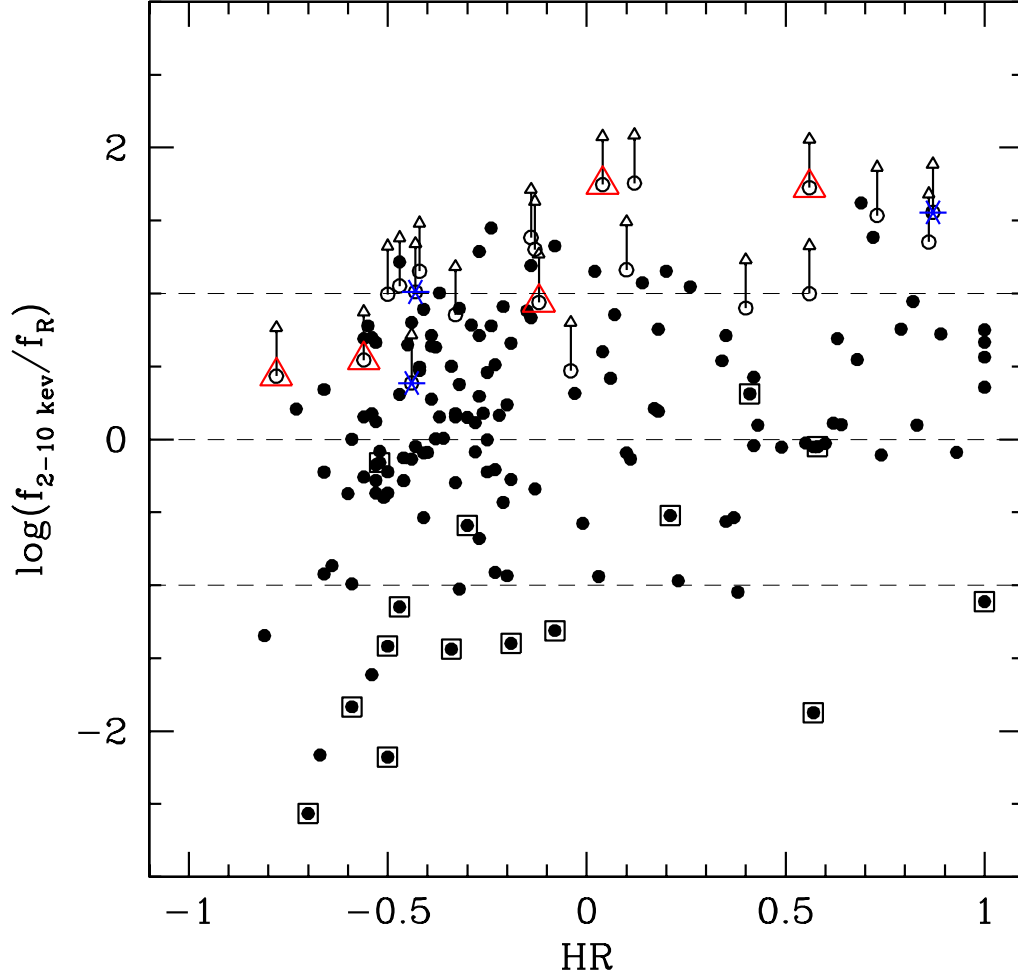


Fig. 9.— X-ray-to-optical flux ratio $\log(f_{2-10\text{keV}}/f_R)$ vs X-ray hardness ratio HR. Lower limits of $\log(f_{2-10\text{keV}}/f_R)$ are plotted for sources without R -band counterparts. Dashed lines show location of constant X-ray-to-optical flux ratio of +1, 0, and -1. Dots enclosed by squares are optically extended sources, open circles enclosed by triangles are R -band nondetected sources which show up in redder bands (I, z'), and stars are bluer bands (B_W, V) detected only.

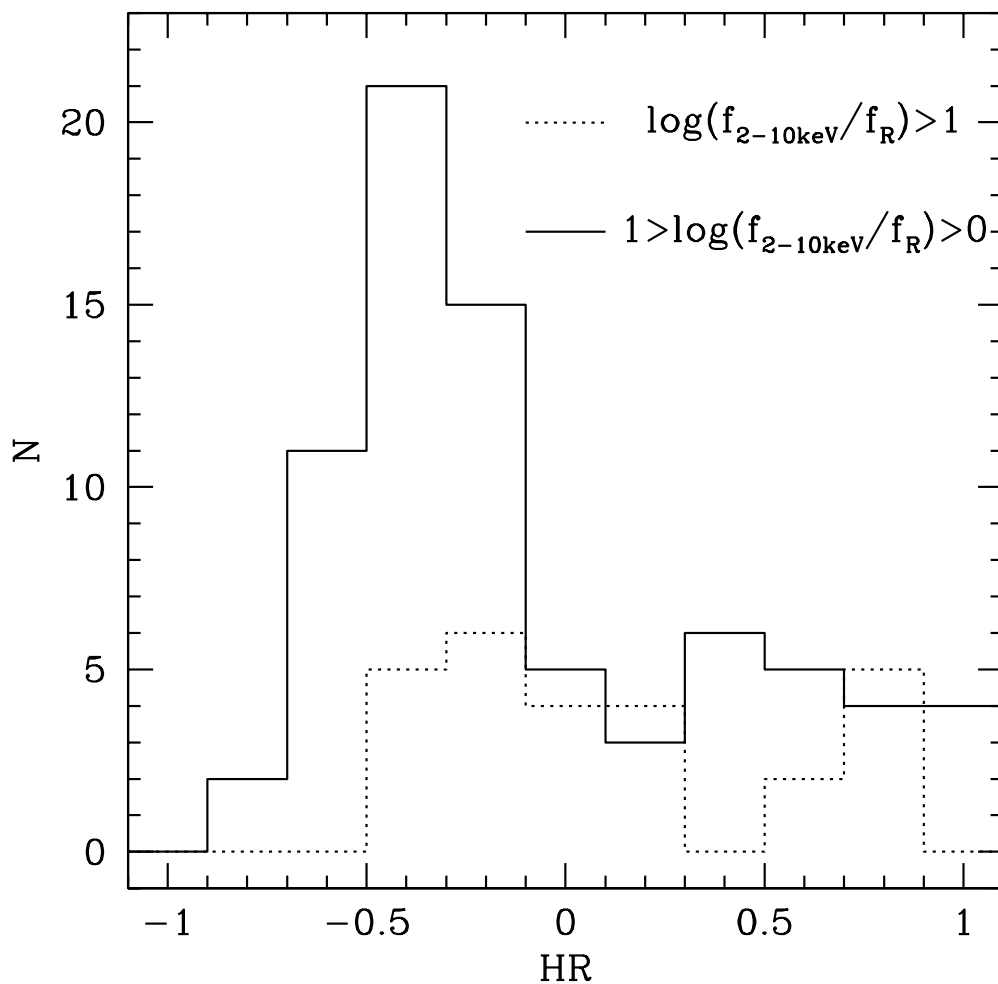


Fig. 10.— Histogram distribution of X-ray hardness ratio for the optically faint X-ray bright sources ($\log(f_{2-10\text{keV}}/f_R) > 1$), comparing with these sources with $1.0 > \log(f_{2-10\text{keV}}/f_R) > 0.0$. The two distributions are distinguishable according to the K-S test at the 98.7% significance level.

Table 1. *Chandra* Sources in LALA Boötes Field

ID	CXOLALA1	RA(J2000)	Dec(J2000)	Err	Tot. Cts.	Soft Cts.	Hard Cts.	det	HR	S _{0.5–10}	S _{0.5–2}	S _{2–10}	Δα(″)	Δδ(″)	R	FWHM(″)
1	J142620.3+353708	14:26:20.36	35:37:08.7	0.2″	4722.9 ^{+71.9} _{-70.8}	3607.8 ^{+62.8} _{-61.8}	1115.2 ^{+35.7} _{-34.6}	TSH	-0.52 ^{+0.01} _{-0.01}	382.34	109.67	212.18	0.3	-0.1	17.54 ± 0.00	1.3
2	J142555.5+353528	14:25:55.50	35:35:28.5	0.5″	32.7 ^{+7.1} _{-5.9}	15.3 ^{+5.2} _{-4.0}	17.4 ^{+5.5} _{-4.3}	TSH	0.07 ^{+0.20} _{-0.20}	3.94	0.69	4.92	0.6	-0.0	24.16 ± 0.12	1.1
3	J142547.2+353627	14:25:47.25	35:36:27.6	0.4″	31.6 ^{+6.9} _{-5.7}	20.0 ^{+5.7} _{-4.5}	11.6 ^{+4.6} _{-3.4}	TSH	-0.27 ^{+0.21} _{-0.19}	2.40	0.57	2.05	0.4	-0.1	21.28 ± 0.01	1.2
4	J142547.1+353954	14:25:47.10	35:39:54.9	0.2″	656.4 ^{+27.4} _{-26.4}	593.6 ^{+26.1} _{-25.0}	62.8 ^{+9.4} _{-8.3}	TSH	-0.81 ^{+0.03} _{-0.02}	48.63	16.50	10.84	0.2	-0.1	17.80 ± 0.00	1.1
5	J142546.4+353522	14:25:46.48	35:35:22.3	0.4″	16.5 ^{+5.5} _{-4.3}	9.0 ^{+4.3} _{-3.1}	7.5 ^{+4.1} _{-2.9}	TSH	-0.08 ^{+0.30} _{-0.29}	1.20	0.25	1.28	0.3	-0.1	20.20 ± 0.01	1.4
6	J142545.3+353449	14:25:45.33	35:34:49.7	0.3″	62.6 ^{+9.3} _{-8.2}	37.4 ^{+7.4} _{-6.3}	25.1 ^{+6.4} _{-5.2}	TSH	-0.19 ^{+0.14} _{-0.14}	4.62	1.04	4.38	0.3	-0.2	23.80 ± 0.08	1.0
7	J142543.3+353548	14:25:43.31	35:35:48.1	0.4″	15.1 ^{+5.3} _{-4.2}	8.7 ^{+4.3} _{-3.1}	6.4 ^{+4.0} _{-2.7}	TSH	-0.15 ^{+0.33} _{-0.30}	1.09	0.24	1.09	-0.1	-0.4	25.86 ± 0.35	0.8
8	J142542.5+353358	14:25:42.53	35:33:58.2	0.4″	30.7 ^{+6.9} _{-5.7}	21.1 ^{+5.8} _{-4.7}	9.6 ^{+4.5} _{-3.3}	TSH	-0.37 ^{+0.21} _{-0.19}	2.79	0.72	2.06	0.4	-0.3	25.48 ± 0.28	0.9
9	J142539.5+353357	14:25:39.55	35:33:57.9	0.4″	34.8 ^{+7.2} _{-6.1}	25.0 ^{+6.3} _{-5.1}	9.8 ^{+4.5} _{-3.3}	TSH	-0.43 ^{+0.19} _{-0.17}	2.58	0.69	1.70	0.2	0.2	>25.7	...
10	J142538.7+353618	14:25:38.72	35:36:18.0	0.4″	9.5 ^{+4.3} _{-3.1}	6.3 ^{+3.8} _{-2.5}	3.2 ^{+3.1} _{-1.7}	TS	-0.32 ^{+0.42} _{-0.33}	0.83	0.21	0.66	-0.0	-0.0	21.64 ± 0.02	1.1
11	J142537.9+353612	14:25:37.94	35:36:12.0	0.3″	25.6 ^{+6.4} _{-5.2}	18.9 ^{+5.6} _{-4.4}	6.6 ^{+4.0} _{-2.7}	TS	-0.47 ^{+0.23} _{-0.19}	1.85	0.51	1.14	0.4	-0.3	20.74 ± 0.01	1.3
12	J142536.3+353634	14:25:36.32	35:36:34.2	0.3″	50.8 ^{+8.5} _{-7.3}	24.0 ^{+6.2} _{-5.0}	26.9 ^{+6.5} _{-5.3}	TSH	0.06 ^{+0.16} _{-0.16}	7.30	1.29	8.96	-0.6	-0.0	22.41 ± 0.03	1.2
13	J142534.7+353407	14:25:34.76	35:34:07.8	0.3″	46.8 ^{+8.2} _{-7.1}	17.6 ^{+5.6} _{-4.4}	29.2 ^{+6.7} _{-5.5}	TSH	0.26 ^{+0.16} _{-0.17}	3.53	0.50	5.19	0.0	-0.1	24.58 ± 0.15	1.0
14	J142533.5+353845	14:25:33.51	35:38:45.6	0.3″	95.9 ^{+11.3} _{-10.2}	63.2 ^{+9.3} _{-8.2}	32.7 ^{+7.2} _{-6.0}	TSH	-0.32 ^{+0.11} _{-0.11}	7.15	1.77	5.66	-0.1	-0.5	22.81 ± 0.04	1.1
15	J142530.7+353911	14:25:30.71	35:39:11.3	0.3″	95.2 ^{+11.2} _{-10.1}	41.7 ^{+7.8} _{-6.7}	53.5 ^{+8.7} _{-7.6}	TSH	0.12 ^{+0.11} _{-0.11}	7.25	1.19	9.46	>25.7	...
16	J142529.2+353412	14:25:29.24	35:34:12.2	0.4″	38.6 ^{+7.7} _{-6.5}	32.1 ^{+7.0} _{-5.8}	6.5 ^{+4.1} _{-2.9}	TS	-0.66 ^{+0.17} _{-0.13}	2.84	0.88	1.11	-0.1	-0.0	21.33 ± 0.01	1.1
17	J142525.4+353622	14:25:25.40	35:36:22.8	0.5″	35.6 ^{+7.3} _{-6.2}	15.9 ^{+5.3} _{-4.2}	19.8 ^{+5.7} _{-4.5}	TSH	0.11 ^{+0.19} _{-0.20}	2.61	0.44	3.35	0.2	-0.1	22.10 ± 0.02	1.1
18	J142520.7+353311	14:25:20.75	35:33:11.7	0.3″	410.9 ^{+22.1} _{-21.0}	300.5 ^{+19.0} _{-17.9}	110.4 ^{+12.1} _{-11.0}	TSH	-0.46 ^{+0.05} _{-0.05}	32.83	8.97	20.55	0.4	-0.3	20.15 ± 0.00	1.0
19	J142614.2+353631	14:26:14.29	35:36:31.5	1.0″	59.4 ^{+9.9} _{-8.8}	46.2 ^{+8.4} _{-7.3}	13.2 ^{+6.1} _{-4.9}	TSH	-0.53 ^{+0.15} _{-0.13}	5.01	1.46	2.61	-0.5	-0.1	24.65 ± 0.08	1.1
20	J142614.2+353833	14:26:14.21	35:38:33.1	0.6″	558.0 ^{+25.7} _{-24.7}	411.4 ^{+22.0} _{-21.0}	146.6 ^{+14.1} _{-13.0}	TSH	-0.47 ^{+0.04} _{-0.04}	44.21	12.24	27.22	0.5	-0.0	20.93 ± 0.01	1.0
21	J142609.5+353213	14:26:09.56	35:32:13.8	0.7″	246.2 ^{+17.8} _{-16.7}	171.2 ^{+14.7} _{-13.6}	75.0 ^{+10.8} _{-9.7}	TSH	-0.39 ^{+0.07} _{-0.07}	20.91	5.46	14.97	0.0	-0.1	22.41 ± 0.03	1.0
22	J142607.6+353351	14:26:07.66	35:33:51.4	0.6″	265.1 ^{+18.1} _{-17.0}	24.3 ^{+6.6} _{-5.4}	240.8 ^{+17.2} _{-16.1}	TSH	0.82 ^{+0.04} _{-0.04}	20.72	0.71	44.35	0.6	0.1	22.00 ± 0.02 ^a	...
23	J142605.8+353508	14:26:05.83	35:35:08.7	0.4″	246.5 ^{+17.4} _{-16.3}	154.4 ^{+13.9} _{-12.8}	92.0 ^{+11.1} _{-10.0}	TSH	-0.25 ^{+0.07} _{-0.07}	19.39	4.56	16.88	0.1	-0.1	20.12 ± 0.00	1.0
24	J142602.4+353605	14:26:02.42	35:36:05.6	0.6″	81.7 ^{+10.7} _{-9.6}	61.5 ^{+9.2} _{-8.1}	20.2 ^{+6.2} _{-5.0}	TSH	-0.50 ^{+0.12} _{-0.11}	6.50	1.84	3.74	-0.1	-0.0	21.40 ± 0.01	1.1
25	J142601.1+354151	14:26:01.18	35:41:51.1	0.7″	284.1 ^{+18.9} _{-17.8}	179.4 ^{+15.1} _{-14.0}	104.8 ^{+12.1} _{-11.0}	TSH	-0.26 ^{+0.06} _{-0.06}	22.87	5.42	19.77	0.5	-0.7	20.96 ± 0.01	1.1
26	J142557.6+353445	14:25:57.65	35:34:45.9	0.4″	65.5 ^{+9.6} _{-8.5}	40.4 ^{+7.8} _{-6.6}	25.1 ^{+6.4} _{-5.2}	TSH	-0.23 ^{+0.14} _{-0.13}	4.92	1.14	4.43	0.0	0.1	19.86 ± 0.00	1.0
27	J142557.7+353512	14:25:57.70	35:35:12.4	0.9″	13.3 ^{+5.1} _{-3.9}	2.7 ^{+3.1} _{-1.7}	10.6 ^{+4.6} _{-3.4}	TH	0.60 ^{+0.23} _{-0.34}	1.37	0.10	2.58	0.6	-0.5	22.65 ± 0.04	1.1
28	J142556.9+353845	14:25:56.94	35:38:45.1	0.5″	87.6 ^{+11.0} _{-9.9}	58.3 ^{+9.0} _{-7.9}	29.4 ^{+7.0} _{-5.8}	TSH	-0.39 ^{+0.12} _{-0.11}	6.54	1.63	5.12	0.2	-0.3	22.42 ± 0.03	1.0
29	J142556.3+354018	14:25:56.34	35:40:18.4	0.5″	132.0 ^{+13.1} _{-12.0}	100.1 ^{+11.5} _{-10.3}	31.8 ^{+7.2} _{-6.1}	TSH	-0.51 ^{+0.09} _{-0.08}	10.61	3.02	5.98	-0.0	-0.2	20.81 ± 0.02	1.0
30	J142555.9+353240	14:25:55.95	35:32:40.6	0.5″	89.4 ^{+11.1} _{-10.0}	55.2 ^{+8.9} _{-7.8}	34.2 ^{+7.4} _{-6.3}	TSH	-0.23 ^{+0.12} _{-0.11}	6.83	1.58	6.13	0.1	0.2	23.06 ± 0.05	1.0
31	J142555.4+353650	14:25:55.40	35:36:50.4	0.7″	15.3 ^{+5.5} _{-4.3}	11.9 ^{+4.8} _{-3.6}	3.4 ^{+3.6} _{-2.3}	TS	-0.56 ^{+0.33} _{-0.25}	1.13	0.33	0.58	0.4	-0.4	>25.7	...
32	J142554.1+353237	14:25:54.11	35:32:37.1	0.5″	95.7 ^{+11.2} _{-10.1}	52.1 ^{+8.5} _{-7.4}	43.6 ^{+8.0} _{-6.9}	TSH	-0.08 ^{+0.11} _{-0.11}	7.29	1.49	7.79	-0.1	-0.4	24.84 ± 0.10	0.9
33	J142553.8+353826	14:25:53.80	35:38:26.0	0.6″	23.6 ^{+6.4} _{-5.2}	14.8 ^{+5.2} _{-4.0}	8.8 ^{+4.5} _{-3.3}	TSH	-0.25 ^{+0.26} _{-0.23}	1.75	0.41	1.53	-0.5	-0.5	24.44 ± 0.10	0.8
34	J142553.6+353314	14:25:53.68	35:33:14.9	0.3″	95.8 ^{+11.3} _{-10.2}	76.7 ^{+10.1} _{-9.0}	19.1 ^{+5.8} _{-4.7}	TSH	-0.60 ^{+0.10} _{-0.09}	7.83	2.35	3.67	-0.0	-0.2	21.41 ± 0.01	1.0

Table 1—Continued

ID	CXOLALA1	RA(J2000)	Dec(J2000)	Err	Tot. Cts.	Soft Cts.	Hard Cts.	det	HR	S _{0.5–10}	S _{0.5–2}	S _{2–10}	Δα(")	Δδ(")	R	FWHM(")
35	J142552.7+353448	14:25:52.72	35:34:48.2	0.7''	10.0 ^{+4.6} _{-3.4}	7.7 ^{+4.1} _{-2.9}	2.2 ^{+3.1} _{-1.7}	TS	-0.54 ^{+0.43} _{-0.30}	0.74	0.21	0.39	-0.3	0.2	25.21 ± 0.27	1.1
36	J142552.4+353730	14:25:52.45	35:37:30.3	0.5''	15.2 ^{+5.5} _{-4.3}	10.6 ^{+4.6} _{-3.4}	4.6 ^{+3.8} _{-2.5}	TS	-0.39 ^{+0.34} _{-0.28}	1.11	0.29	0.78	-1.1	-0.6	25.80 ± 0.27	1.3
37	J142552.2+353823	14:25:52.27	35:38:23.7	0.4''	53.4 ^{+8.8} _{-7.7}	7.4 ^{+4.1} _{-2.9}	46.0 ^{+8.2} _{-7.1}	TH	0.72 ^{+0.10} _{-0.13}	4.10	0.21	8.23 ^b	...
38	J142551.3+353404	14:25:51.38	35:34:04.4	0.4''	37.1 ^{+7.6} _{-6.5}	31.7 ^{+7.0} _{-5.8}	5.5 ^{+4.0} _{-2.7}	TS	-0.70 ^{+0.17} _{-0.13}	2.77	0.88	0.96	0.1	-0.1	17.38 ± 0.00	1.3
39	J142551.0+353307	14:25:51.00	35:33:07.2	0.8''	23.2 ^{+6.5} _{-5.3}	16.2 ^{+5.5} _{-4.3}	7.0 ^{+4.3} _{-3.1}	TS	-0.39 ^{+0.26} _{-0.23}	1.80	0.47	1.28	0.0	-0.6	24.17 ± 0.11	1.0
40	J142550.8+353033	14:25:50.81	35:30:33.6	1.0''	71.0 ^{+10.3} _{-9.2}	58.9 ^{+9.2} _{-8.1}	12.1 ^{+5.6} _{-4.4}	TSH	-0.66 ^{+0.13} _{-0.11}	5.73	1.78	2.28	0.2	-0.2	22.29 ± 0.03	1.0
41	J142550.6+353743	14:25:50.67	35:37:43.1	0.5''	18.4 ^{+5.8} _{-4.7}	13.8 ^{+5.1} _{-3.9}	4.6 ^{+3.8} _{-2.5}	TS	-0.50 ^{+0.29} _{-0.23}	1.34	0.38	0.79	0.1	-0.0	23.45 ± 0.06	1.0
42	J142550.4+353247	14:25:50.49	35:32:47.9	0.8''	26.1 ^{+6.7} _{-5.5}	20.1 ^{+5.8} _{-4.7}	6.0 ^{+4.1} _{-2.9}	TS	-0.53 ^{+0.24} _{-0.19}	2.06	0.60	1.12	0.0	-0.1	22.93 ± 0.05	1.0
43	J142549.9+353203	14:25:49.90	35:32:03.8	0.5''	91.9 ^{+11.1} _{-10.0}	65.1 ^{+9.4} _{-8.3}	26.8 ^{+6.7} _{-5.5}	TSH	-0.41 ^{+0.11} _{-0.10}	7.82	2.07	5.37	0.1	-0.1	21.69 ± 0.02	1.1
44	J142549.8+353619	14:25:49.81	35:36:19.0	0.6''	9.0 ^{+4.5} _{-3.3}	0.3 ^{+4.3} _{-0.3}	8.7 ^{+4.3} _{-3.1}	TH	0.93 ^{+0.06} _{-0.40}	0.69	0.01	1.55	0.6	-0.4	23.05 ± 0.07	1.1
45	J142549.2+353615	14:25:49.26	35:36:15.3	0.6''	8.5 ^{+4.5} _{-3.3}	6.1 ^{+4.0} _{-2.7}	2.4 ^{+3.1} _{-1.7}	TS	-0.44 ^{+0.48} _{-0.35}	0.62	0.17	0.40	0.3	0.1	>25.7	...
46	J142548.5+353507	14:25:48.58	35:35:07.8	0.4''	29.3 ^{+6.8} _{-5.6}	14.5 ^{+5.1} _{-3.9}	14.8 ^{+5.2} _{-4.0}	TSH	0.02 ^{+0.21} _{-0.22}	2.14	0.40	2.55	-0.1	-0.4	25.61 ± 0.32	1.4
47	J142548.2+353041	14:25:48.21	35:30:41.1	0.4''	162.2 ^{+14.4} _{-13.3}	103.1 ^{+11.7} _{-10.6}	59.1 ^{+9.2} _{-8.1}	TSH	-0.27 ^{+0.09} _{-0.08}	12.86	3.06	10.98	0.2	0.1	24.37 ± 0.10	0.7
48	J142547.6+353043	14:25:47.67	35:30:43.0	0.7''	26.4 ^{+7.2} _{-6.0}	7.6 ^{+4.5} _{-3.3}	18.8 ^{+6.2} _{-5.0}	TH	0.43 ^{+0.21} _{-0.25}	2.14	0.23	3.57	0.3	-0.4	22.61 ± 0.04	1.1
49	J142547.2+353728	14:25:47.25	35:37:28.0	0.9''	6.1 ^{+3.8} _{-2.5}	3.2 ^{+3.1} _{-1.7}	2.9 ^{+3.1} _{-1.7}	T	-0.04 ^{+0.50} _{-0.49}	0.44	0.09	0.49	>25.7	...
50	J142546.9+353240	14:25:46.95	35:32:40.3	0.5''	55.4 ^{+8.8} _{-7.7}	44.3 ^{+8.0} _{-6.9}	11.1 ^{+4.6} _{-3.4}	TSH	-0.59 ^{+0.14} _{-0.11}	4.27	1.28	2.01	-0.0	-0.4	18.41 ± 0.00	2.0
51	J142546.3+353349	14:25:46.33	35:33:49.4	0.8''	11.8 ^{+4.9} _{-3.7}	2.6 ^{+3.1} _{-1.7}	9.2 ^{+4.5} _{-3.3}	T	0.56 ^{+0.26} _{-0.37}	0.90	0.07	1.65	>25.7	...
52	J142546.1+353354	14:25:46.13	35:33:54.9	0.4''	17.7 ^{+5.6} _{-4.4}	10.0 ^{+4.5} _{-3.3}	7.7 ^{+4.1} _{-2.9}	TSH	-0.12 ^{+0.29} _{-0.28}	1.41	0.30	1.44	0.1	-0.6	>25.7	...
53	J142546.0+353826	14:25:46.02	35:38:26.3	0.5''	25.0 ^{+6.4} _{-5.2}	10.0 ^{+4.5} _{-3.3}	15.0 ^{+5.2} _{-4.0}	TSH	0.20 ^{+0.22} _{-0.24}	1.95	0.29	2.71	0.3	-0.8	25.55 ± 0.27	0.9
54	J142545.8+353849	14:25:45.85	35:38:49.2	0.4''	29.1 ^{+6.9} _{-5.7}	18.9 ^{+5.6} _{-4.4}	10.2 ^{+4.8} _{-3.6}	TSH	-0.30 ^{+0.22} _{-0.20}	2.23	0.54	1.81	0.6	-0.3	21.63 ± 0.02	1.4
55	J142545.7+353228	14:25:45.78	35:32:28.4	0.7''	20.4 ^{+6.1} _{-4.9}	20.6 ^{+5.8} _{-4.7}	0.0 ^{+2.8} _{-0.0}	TS	-1.00 ^{+0.21} _{-0.00}	1.54	0.58	< 0.49	0.1	-0.2	20.28 ± 0.00	1.0
56	J142545.6+353152	14:25:45.69	35:31:52.9	0.4''	91.9 ^{+11.3} _{-10.2}	63.9 ^{+9.4} _{-8.3}	28.0 ^{+7.1} _{-5.9}	TSH	-0.38 ^{+0.12} _{-0.11}	7.30	1.90	5.24	-0.1	-0.0	21.96 ± 0.02	1.0
57	J142545.1+353616	14:25:45.17	35:36:16.3	0.8''	6.3 ^{+3.8} _{-2.5}	2.1 ^{+2.8} _{-1.4}	4.2 ^{+3.3} _{-2.0}	T	0.34 ^{+0.39} _{-0.52}	0.62	0.08	0.97	0.2	-0.5	25.13 ± 0.24	1.2
58	J142544.7+353954	14:25:44.70	35:39:54.1	0.8''	23.2 ^{+6.4} _{-5.2}	13.8 ^{+5.2} _{-4.0}	9.3 ^{+4.5} _{-3.3}	TSH	-0.19 ^{+0.26} _{-0.24}	1.71	0.38	1.61	0.0	-0.2	22.55 ± 0.03	1.0
59	J142541.6+354107	14:25:41.66	35:41:07.2	0.7''	35.3 ^{+7.8} _{-6.6}	24.4 ^{+6.5} _{-5.3}	10.8 ^{+5.1} _{-3.9}	TS	-0.38 ^{+0.21} _{-0.18}	2.79	0.73	2.01	0.4	0.5	24.57 ± 0.19	1.1
60	J142538.7+353342	14:25:38.73	35:33:42.1	0.4''	14.5 ^{+5.3} _{-4.2}	7.4 ^{+4.0} _{-2.7}	7.2 ^{+4.3} _{-3.1}	TSH	-0.01 ^{+0.33} _{-0.33}	1.08	0.21	1.26	-0.0	-0.3	22.06 ± 0.02	1.1
61	J142538.5+353429	14:25:38.51	35:34:29.9	0.4''	19.4 ^{+5.9} _{-4.8}	4.3 ^{+3.6} _{-2.3}	15.2 ^{+5.3} _{-4.2}	TH	0.57 ^{+0.20} _{-0.27}	1.42	0.12	2.61	0.2	-0.4	22.58 ± 0.03	1.0
62	J142538.2+353438	14:25:38.29	35:34:38.0	0.4''	21.6 ^{+5.9} _{-4.8}	14.7 ^{+5.1} _{-3.9}	6.9 ^{+4.0} _{-2.7}	TSH	-0.36 ^{+0.26} _{-0.22}	1.61	0.41	1.21	0.2	-0.2	23.56 ± 0.07	1.1
63	J142537.1+354309	14:25:37.15	35:43:09.8	1.3''	44.6 ^{+9.1} _{-8.0}	34.9 ^{+7.7} _{-6.5}	9.7 ^{+5.7} _{-4.5}	TS	-0.56 ^{+0.19} _{-0.16}	3.60	1.06	1.84	0.5	-0.4	23.47 ± 0.07	1.1
64	J142536.9+353209	14:25:36.99	35:32:09.3	0.4''	59.0 ^{+9.3} _{-8.2}	41.7 ^{+7.8} _{-6.7}	17.3 ^{+5.8} _{-4.7}	TSH	-0.41 ^{+0.15} _{-0.13}	4.58	1.21	3.16	0.4	-0.3	24.73 ± 0.18	1.1
65	J142535.9+354107	14:25:35.99	35:41:07.1	0.3''	393.0 ^{+21.6} _{-20.5}	275.1 ^{+18.1} _{-17.1}	117.9 ^{+12.4} _{-11.3}	TSH	-0.40 ^{+0.05} _{-0.05}	30.39	7.99	21.31	0.2	-0.2	20.20 ± 0.01	1.0
66	J142534.5+353551	14:25:34.52	35:35:51.3	0.4''	8.2 ^{+4.1} _{-2.9}	6.3 ^{+3.8} _{-2.5}	1.9 ^{+2.8} _{-1.4}	TS	-0.54 ^{+0.46} _{-0.30}	0.78	0.22	0.41	0.1	0.1	20.68 ± 0.01	1.2
67	J142533.8+354138	14:25:33.80	35:41:38.1	0.7''	96.8 ^{+11.6} _{-10.5}	70.9 ^{+10.0} _{-8.9}	25.8 ^{+6.7} _{-5.5}	TSH	-0.46 ^{+0.11} _{-0.10}	8.23	2.27	5.15	-0.1	-0.3	21.26 ± 0.02	1.0
68	J142533.0+353648	14:25:33.09	35:36:48.5	0.5''	18.2 ^{+5.6} _{-4.4}	13.2 ^{+4.9} _{-3.7}	5.0 ^{+3.6} _{-2.3}	TSH	-0.45 ^{+0.28} _{-0.22}	2.20	0.60	1.40	0.2	-0.0	25.00 ± 0.21	0.8

Table 1—Continued

ID	CXOLALA1	RA(J2000)	Dec(J2000)	Err	Tot. Cts.	Soft Cts.	Hard Cts.	det	HR	S _{0.5–10}	S _{0.5–2}	S _{2–10}	$\Delta\alpha(^{\prime\prime})$	$\Delta\delta(^{\prime\prime})$	R	FWHM(^{\prime\prime})
69	J142531.1+353921	14:25:31.17	35:39:21.6	0.6''	36.4 ^{+7.6} _{-6.5}	4.9 ^{+3.8} _{-2.5}	31.5 ^{+7.1} _{-5.9}	TH	0.73 ^{+0.12} _{-0.17}	2.82	0.14	5.68	>25.7	...
70	J142530.6+353420	14:25:30.63	35:34:20.3	0.3''	48.3 ^{+8.3} _{-7.2}	34.5 ^{+7.2} _{-6.0}	13.8 ^{+5.1} _{-3.9}	TSH	-0.42 ^{+0.16} _{-0.14}	3.53	0.94	2.36	>25.7	...
71	J142529.9+353640	14:25:29.91	35:36:40.0	0.4''	16.9 ^{+5.5} _{-4.3}	12.9 ^{+4.9} _{-3.7}	4.0 ^{+3.3} _{-2.0}	TS	-0.53 ^{+0.29} _{-0.22}	1.29	0.37	0.70	0.1	-0.5	25.80 ± 0.29	0.8
72	J142529.2+353248	14:25:29.22	35:32:48.4	0.4''	40.4 ^{+7.8} _{-6.7}	29.8 ^{+6.9} _{-5.7}	10.6 ^{+4.6} _{-3.4}	TSH	-0.47 ^{+0.18} _{-0.15}	3.04	0.84	1.87	>25.7	...
73	J142526.6+353140	14:25:26.68	35:31:40.8	0.8''	42.3 ^{+8.2} _{-7.0}	24.1 ^{+6.4} _{-5.2}	18.1 ^{+5.8} _{-4.7}	TSH	-0.13 ^{+0.19} _{-0.18}	3.29	0.70	3.32	>25.7	...
74	J142525.7+353841	14:25:25.72	35:38:41.5	0.4''	62.8 ^{+9.4} _{-8.3}	8.7 ^{+4.3} _{-3.1}	54.1 ^{+8.8} _{-7.6}	TSH	0.72 ^{+0.09} _{-0.12}	4.66	0.24	9.33	0.6	-0.5	24.79 ± 0.25	1.9
75	J142524.7+353037	14:25:24.70	35:30:37.1	0.5''	151.2 ^{+14.0} _{-12.9}	117.3 ^{+12.3} _{-11.2}	33.9 ^{+7.5} _{-6.4}	TSH	-0.54 ^{+0.08} _{-0.07}	12.30	3.57	6.49	0.7	0.1	23.46 ± 0.07	1.1
76	J142523.6+352824	14:25:23.69	35:28:24.5	0.7''	301.7 ^{+19.1} _{-18.0}	58.9 ^{+9.1} _{-8.0}	242.8 ^{+17.2} _{-16.1}	TSH	0.62 ^{+0.05} _{-0.05}	85.17	6.21	161.16	0.2	-0.1	18.51 ± 0.00	1.1
77	J142521.8+353407	14:25:21.87	35:34:07.8	0.5''	35.3 ^{+7.5} _{-6.4}	20.1 ^{+5.8} _{-4.7}	15.2 ^{+5.5} _{-4.3}	TSH	-0.14 ^{+0.20} _{-0.20}	2.78	0.59	2.78	0.1	-0.4	25.61 ± 0.29	1.0
78	J142521.3+353029	14:25:21.38	35:30:29.5	0.9''	51.6 ^{+9.2} _{-8.1}	15.1 ^{+5.7} _{-4.5}	36.5 ^{+7.8} _{-6.7}	TSH	0.42 ^{+0.15} _{-0.17}	4.26	0.47	7.06	-0.4	-0.2	21.52 ± 0.01	1.1
79	J142517.7+353822	14:25:17.70	35:38:22.2	0.7''	37.3 ^{+7.6} _{-6.5}	22.2 ^{+6.1} _{-4.9}	15.1 ^{+5.3} _{-4.2}	TSH	-0.19 ^{+0.19} _{-0.18}	2.83	0.63	2.67	0.5	-0.3	19.19 ± 0.00	1.8
80	J142514.3+353918	14:25:14.37	35:39:18.2	0.6''	118.5 ^{+12.6} _{-11.5}	71.7 ^{+9.9} _{-8.8}	46.8 ^{+8.5} _{-7.4}	TSH	-0.21 ^{+0.10} _{-0.10}	9.17	2.09	8.45	0.5	-0.9	23.71 ± 0.09	1.2
81	J142514.3+353618	14:25:14.34	35:36:18.8	0.4''	102.9 ^{+11.7} _{-10.6}	82.2 ^{+10.4} _{-9.3}	20.7 ^{+6.2} _{-5.0}	TSH	-0.59 ^{+0.10} _{-0.09}	7.83	2.34	3.68	0.1	-0.2	19.86 ± 0.00	1.2
82	J142513.1+353323	14:25:13.18	35:33:23.4	0.6''	98.5 ^{+11.8} _{-10.7}	73.9 ^{+10.2} _{-9.1}	24.6 ^{+6.7} _{-5.5}	TSH	-0.50 ^{+0.11} _{-0.10}	8.18	2.30	4.77	0.4	-0.3	18.51 ± 0.00	1.4
83	J142512.0+353124	14:25:12.00	35:31:24.3	0.7''	214.7 ^{+16.5} _{-15.5}	165.1 ^{+14.5} _{-13.4}	49.5 ^{+8.8} _{-7.7}	TSH	-0.53 ^{+0.07} _{-0.06}	17.70	5.09	9.57	0.6	0.1	20.86 ± 0.01	1.0
84	J142511.3+353857	14:25:11.32	35:38:57.8	0.6''	121.6 ^{+12.9} _{-11.8}	89.7 ^{+11.0} _{-9.9}	31.9 ^{+7.6} _{-6.5}	TSH	-0.47 ^{+0.10} _{-0.09}	9.49	2.63	5.82	-0.2	0.2	24.88 ± 0.26	1.5
85	J142509.3+354356	14:25:09.39	35:43:56.1	1.1''	349.8 ^{+21.1} _{-20.0}	267.4 ^{+18.3} _{-17.2}	82.5 ^{+11.4} _{-10.3}	TSH	-0.52 ^{+0.05} _{-0.05}	41.92	12.05	23.30	0.2	-0.6	20.13 ± 0.01	1.2
86	J142504.5+354107	14:25:04.58	35:41:07.9	0.6''	473.1 ^{+23.9} _{-22.8}	338.3 ^{+20.2} _{-19.1}	134.9 ^{+13.5} _{-12.4}	TSH	-0.42 ^{+0.05} _{-0.04}	41.21	11.08	27.65	0.6	0.3	21.39 ± 0.01	1.1
87	J142457.1+353518	14:24:57.16	35:35:18.8	0.9''	257.4 ^{+18.2} _{-17.1}	197.9 ^{+15.8} _{-14.7}	59.6 ^{+9.9} _{-8.8}	TSH	-0.53 ^{+0.06} _{-0.06}	24.83	7.15	13.52	0.5	-0.7	20.00 ± 0.00	1.0
88	J142618.8+354218	14:26:18.84	35:42:18.4	1.5''	227.6 ^{+17.8} _{-16.7}	156.9 ^{+14.4} _{-13.3}	70.7 ^{+11.1} _{-10.0}	TSH	-0.37 ^{+0.07} _{-0.07}	26.93	6.97	19.76	0.9	0.1	20.89 ± 0.01	1.1
89	J142618.6+353754	14:26:18.60	35:37:54.2	2.2''	39.8 ^{+9.4} _{-8.3}	9.1 ^{+5.2} _{-4.0}	30.7 ^{+8.3} _{-7.2}	TH	0.55 ^{+0.17} _{-0.21}	3.24	0.28	5.86	-0.3	-0.7	21.77 ± 0.02	1.2
90	J142611.9+354230	14:26:11.92	35:42:30.5	1.7''	80.0 ^{+12.1} _{-11.0}	62.4 ^{+9.9} _{-8.8}	17.6 ^{+7.8} _{-6.6}	TS	-0.56 ^{+0.14} _{-0.13}	9.28	2.72	4.80	0.6	-0.0	21.40 ± 0.01	1.0
91	J142610.8+354202	14:26:10.89	35:42:02.5	1.5''	151.9 ^{+14.8} _{-13.7}	45.4 ^{+7.8} _{-7.6}	106.6 ^{+12.4} _{-11.3}	TSH	0.41 ^{+0.08} _{-0.09}	17.47	1.96	28.81	1.1	-0.2	20.88 ± 0.02	1.3
92	J142606.7+353151	14:26:06.72	35:31:51.3	1.5''	50.3 ^{+9.3} _{-8.2}	36.2 ^{+7.8} _{-6.6}	14.0 ^{+5.9} _{-4.8}	TS	-0.44 ^{+0.18} _{-0.16}	4.00	1.08	2.63	-0.3	0.3	24.70 ± 0.21	1.1
93	J142604.7+353015	14:26:04.78	35:30:15.3	1.7''	75.8 ^{+11.0} _{-9.9}	34.6 ^{+7.6} _{-6.5}	41.3 ^{+8.5} _{-7.4}	TSH	0.10 ^{+0.14} _{-0.14}	6.90	1.18	8.84	1.1	-0.2	21.15 ± 0.01	1.2
94	J142603.7+353246	14:26:03.73	35:32:46.2	1.6''	15.0 ^{+6.2} _{-5.0}	6.0 ^{+4.1} _{-2.9}	9.0 ^{+5.2} _{-4.0}	T	0.21 ^{+0.34} _{-0.38}	1.24	0.19	1.75	-0.4	0.1	21.83 ± 0.02	1.3
95	J142600.2+353442	14:26:00.24	35:34:42.4	0.8''	17.3 ^{+5.7} _{-4.5}	0.0 ^{+1.9} _{-0.0}	18.3 ^{+5.7} _{-4.5}	TH	1.00 ^{+0.00} _{-0.18}	1.34	< 0.06	3.31	0.3	-0.6	24.33 ± 0.13	1.1
96	J142558.1+353216	14:25:58.13	35:32:16.1	1.5''	19.6 ^{+6.3} _{-5.1}	13.1 ^{+5.2} _{-4.0}	6.5 ^{+4.3} _{-3.1}	TS	-0.33 ^{+0.30} _{-0.26}	1.52	0.38	1.18	>25.7	...
97	J142552.4+352724	14:25:52.47	35:27:24.1	1.8''	88.1 ^{+11.9} _{-10.8}	50.6 ^{+8.8} _{-7.7}	37.5 ^{+8.6} _{-7.5}	TSH	-0.14 ^{+0.13} _{-0.13}	10.55	2.27	10.58	-0.6	-0.5	23.27 ± 0.08	1.0
98	J142551.4+353433	14:25:51.43	35:34:33.1	0.7''	9.6 ^{+4.5} _{-3.3}	0.0 ^{+1.9} _{-0.0}	9.8 ^{+4.5} _{-3.3}	TH	1.00 ^{+0.00} _{-0.31}	0.71	< 0.05	1.72	0.1	-0.1	24.57 ± 0.18	1.3
99	J142551.1+353015	14:25:51.16	35:30:15.7	1.5''	20.6 ^{+6.9} _{-5.7}	16.1 ^{+5.7} _{-4.5}	4.5 ^{+4.6} _{-3.4}	TS	-0.56 ^{+0.32} _{-0.26}	1.62	0.48	0.83	0.1	0.2	25.68 ± 0.28	0.9
100	J142547.4+352720	14:25:47.43	35:27:20.2	1.4''	179.7 ^{+15.9} _{-14.8}	127.4 ^{+13.1} _{-12.0}	52.3 ^{+9.8} _{-8.7}	TSH	-0.41 ^{+0.08} _{-0.08}	15.14	4.03	10.38	0.4	-0.3	19.87 ± 0.00	1.0
101	J142545.5+353003	14:25:45.53	35:30:03.6	1.3''	22.8 ^{+6.8} _{-5.6}	11.7 ^{+4.9} _{-3.7}	11.0 ^{+5.3} _{-4.2}	TS	-0.03 ^{+0.27} _{-0.28}	1.85	0.36	2.11	0.7	0.6	23.73 ± 0.09	1.0
102	J142544.7+354046	14:25:44.77	35:40:46.6	1.1''	20.4 ^{+6.1} _{-4.9}	6.4 ^{+4.0} _{-2.7}	14.0 ^{+5.2} _{-4.0}	TH	0.38 ^{+0.23} _{-0.28}	1.61	0.19	2.61	0.1	-0.7	20.09 ± 0.01	1.2

Table 1—Continued

ID	CXOLALA1	RA(J2000)	Dec(J2000)	Err	Tot. Cts.	Soft Cts.	Hard Cts.	det	HR	S _{0.5–10}	S _{0.5–2}	S _{2–10}	$\Delta\alpha(^{\prime\prime})$	$\Delta\delta(^{\prime\prime})$	R	FWHM(^{\prime\prime})
103	J142544.2+354018	14:25:44.20	35:40:18.4	0.9''	22.7 ^{+6.2} _{-5.0}	1.6 ^{+2.8} _{-1.4}	21.1 ^{+5.9} _{-4.8}	TH	0.86 ^{+0.10} _{-0.20}	1.72	0.05	3.74	>25.7	...
104	J142541.8+354249	14:25:41.80	35:42:49.7	1.3''	42.3 ^{+8.4} _{-7.3}	24.1 ^{+6.4} _{-5.2}	18.2 ^{+6.2} _{-5.0}	TSH	-0.13 ^{+0.19} _{-0.18}	3.64	0.78	3.68	-0.9	0.6	21.49 ± 0.02	1.2
105	J142539.6+353942	14:25:39.65	35:39:42.6	0.8''	18.3 ^{+5.7} _{-4.5}	11.3 ^{+4.6} _{-3.4}	7.0 ^{+4.1} _{-2.9}	TS	-0.24 ^{+0.29} _{-0.27}	1.37	0.32	1.21	0.4	-0.5	25.49 ± 0.30	1.1
106	J142536.8+353147	14:25:36.81	35:31:47.2	1.0''	11.5 ^{+5.1} _{-3.9}	2.1 ^{+3.1} _{-1.7}	9.3 ^{+4.6} _{-3.4}	TH	0.63 ^{+0.25} _{-0.39}	0.91	0.06	1.73	0.2	-0.2	24.88 ± 0.21	2.0
107	J142533.3+353130	14:25:33.33	35:31:30.6	0.8''	20.7 ^{+6.4} _{-5.2}	5.3 ^{+3.8} _{-2.5}	15.4 ^{+5.7} _{-4.5}	TH	0.49 ^{+0.22} _{-0.28}	1.59	0.15	2.78	0.5	-0.2	22.50 ± 0.03	1.0
108	J142532.6+352838	14:25:32.66	35:28:38.8	1.4''	39.5 ^{+9.0} _{-7.9}	32.9 ^{+7.7} _{-6.5}	6.6 ^{+5.5} _{-4.3}	TS	-0.66 ^{+0.21} _{-0.17}	3.21	1.00	1.26	0.9	0.9	24.35 ± 0.17	1.4
109	J142531.4+354452	14:25:31.41	35:44:52.5	2.1''	62.7 ^{+10.8} _{-9.7}	20.7 ^{+6.5} _{-5.3}	42.0 ^{+9.2} _{-8.1}	TSH	0.35 ^{+0.15} _{-0.16}	5.35	0.66	8.49	-0.0	1.4	20.02 ± 0.00	1.2
110	J142530.8+353208	14:25:30.82	35:32:08.6	1.1''	10.3 ^{+4.5} _{-3.3}	5.0 ^{+3.6} _{-2.3}	5.3 ^{+3.6} _{-2.3}	T	0.03 ^{+0.37} _{-0.38}	1.31	0.24	1.58	-0.1	-0.4	20.91 ± 0.01	1.2
111	J142528.2+353958	14:25:28.24	35:39:58.4	0.9''	21.1 ^{+6.2} _{-5.0}	3.8 ^{+3.6} _{-2.3}	17.3 ^{+5.6} _{-4.4}	TH	0.64 ^{+0.19} _{-0.26}	1.58	0.11	3.01	0.5	-0.3	22.81 ± 0.04	1.0
112	J142527.5+354012	14:25:27.59	35:40:12.1	0.8''	24.6 ^{+6.8} _{-5.6}	11.2 ^{+4.8} _{-3.6}	13.5 ^{+5.5} _{-4.3}	TSH	0.10 ^{+0.25} _{-0.26}	1.89	0.32	2.41	>25.7	...
113	J142527.4+353101	14:25:27.49	35:31:01.0	1.2''	12.7 ^{+5.6} _{-4.4}	8.6 ^{+4.6} _{-3.4}	4.1 ^{+4.0} _{-2.7}	TS	-0.34 ^{+0.40} _{-0.35}	1.06	0.27	0.81	0.4	-0.1	20.38 ± 0.02	1.3
114	J142526.6+353327	14:25:26.66	35:33:27.2	0.7''	10.8 ^{+4.9} _{-3.7}	8.3 ^{+4.3} _{-3.1}	2.5 ^{+3.3} _{-2.0}	TS	-0.53 ^{+0.42} _{-0.31}	0.84	0.24	0.46	-1.0	-0.1	24.91 ± 0.15	1.2
115	J142524.2+352928	14:25:24.22	35:29:28.6	1.4''	44.8 ^{+9.0} _{-7.9}	25.9 ^{+6.7} _{-5.5}	18.9 ^{+6.7} _{-5.5}	TSH	-0.14 ^{+0.19} _{-0.19}	4.00	0.86	4.01	>25.7	...
116	J142523.8+354122	14:25:23.80	35:41:22.4	0.8''	52.7 ^{+9.2} _{-8.1}	41.9 ^{+8.0} _{-6.9}	10.8 ^{+5.3} _{-4.2}	TS	-0.59 ^{+0.16} _{-0.13}	4.26	1.27	2.04	0.0	0.2	22.98 ± 0.04	1.0
117	J142523.6+353216	14:25:23.69	35:32:16.7	1.1''	26.5 ^{+6.7} _{-5.5}	11.4 ^{+4.9} _{-3.7}	15.0 ^{+5.2} _{-4.0}	TSH	0.14 ^{+0.23} _{-0.24}	2.06	0.33	2.74	0.6	-0.5	25.34 ± 0.27	0.8
118	J142523.0+354313	14:25:23.00	35:43:13.4	1.1''	104.3 ^{+12.6} _{-11.5}	66.8 ^{+9.8} _{-8.7}	37.5 ^{+8.5} _{-7.4}	TSH	-0.28 ^{+0.12} _{-0.11}	8.28	1.99	7.00	0.3	0.8	21.42 ± 0.02	1.0
119	J142522.8+353116	14:25:22.82	35:31:16.8	1.0''	28.9 ^{+7.1} _{-5.9}	4.6 ^{+3.8} _{-2.5}	24.3 ^{+6.5} _{-5.3}	TH	0.68 ^{+0.15} _{-0.21}	2.44	0.15	4.79	0.7	-0.2	23.41 ± 0.07	1.1
120	J142522.4+353517	14:25:22.40	35:35:17.2	0.6''	10.6 ^{+4.8} _{-3.6}	3.2 ^{+3.3} _{-2.0}	7.4 ^{+4.1} _{-2.9}	T	0.40 ^{+0.32} _{-0.41}	0.81	0.09	1.32	>25.7	...
121	J142521.1+353340	14:25:21.10	35:33:40.0	0.7''	16.3 ^{+5.6} _{-4.4}	14.1 ^{+5.2} _{-4.0}	2.2 ^{+3.1} _{-1.7}	TS	-0.73 ^{+0.29} _{-0.18}	1.59	0.51	0.50	0.0	-0.6	25.03 ± 0.21	1.1
122	J142517.6+353453	14:25:17.61	35:34:53.0	0.5''	19.1 ^{+5.9} _{-4.8}	11.5 ^{+4.8} _{-3.6}	7.6 ^{+4.3} _{-3.1}	TS	-0.20 ^{+0.29} _{-0.27}	1.44	0.33	1.34	0.7	0.3	24.03 ± 0.11	1.0
													-0.2	-1.3	25.08 ± 0.09	1.3
123	J142516.6+354129	14:25:16.67	35:41:29.6	1.3''	45.8 ^{+8.6} _{-7.5}	33.1 ^{+7.2} _{-6.1}	12.7 ^{+5.5} _{-4.3}	TS	-0.44 ^{+0.18} _{-0.16}	3.60	0.98	2.34	0.2	0.1	22.49 ± 0.04	1.2
124	J142516.4+352940	14:25:16.43	35:29:40.7	1.2''	70.9 ^{+10.7} _{-9.6}	47.5 ^{+8.5} _{-7.4}	23.4 ^{+7.2} _{-6.1}	TSH	-0.33 ^{+0.15} _{-0.14}	6.16	1.54	4.78	0.2	0.8	21.31 ± 0.01	1.2
125	J142516.0+353142	14:25:16.00	35:31:42.3	1.1''	11.6 ^{+5.7} _{-4.5}	7.1 ^{+4.3} _{-3.1}	4.5 ^{+4.5} _{-3.3}	T	-0.22 ^{+0.45} _{-0.43}	0.97	0.22	0.89	-0.1	-0.8	24.29 ± 0.16	1.0
126	J142514.9+354004	14:25:14.90	35:40:04.1	0.9''	48.1 ^{+8.9} _{-7.8}	31.3 ^{+7.2} _{-6.0}	16.8 ^{+6.1} _{-4.9}	TSH	-0.30 ^{+0.18} _{-0.16}	3.74	0.92	3.06	1.0	0.2	22.91 ± 0.05	1.2
127	J142510.9+353602	14:25:10.94	35:36:02.8	1.0''	39.7 ^{+8.0} _{-6.9}	16.4 ^{+5.5} _{-4.3}	23.2 ^{+6.5} _{-5.3}	TSH	0.18 ^{+0.18} _{-0.19}	3.08	0.48	4.21	-0.9	0.3	22.67 ± 0.05	1.0
128	J142510.1+353411	14:25:10.19	35:34:11.4	0.9''	50.4 ^{+8.9} _{-7.8}	31.2 ^{+7.1} _{-5.9}	19.2 ^{+6.2} _{-5.0}	TSH	-0.23 ^{+0.17} _{-0.16}	3.94	0.91	3.51	-0.6	0.1	21.87 ± 0.02	1.2
129	J142509.5+354244	14:25:09.51	35:42:44.9	2.1''	71.2 ^{+11.5} _{-10.3}	15.2 ^{+6.3} _{-5.1}	56.0 ^{+10.1} _{-9.0}	TH	0.58 ^{+0.12} _{-0.14}	7.45	0.60	13.80	-0.8	2.0	20.77 ± 0.01	1.4
130	J142509.5+353747	14:25:09.50	35:37:47.5	0.6''	110.9 ^{+12.4} _{-11.3}	32.6 ^{+7.2} _{-6.1}	78.3 ^{+10.6} _{-9.5}	TSH	0.42 ^{+0.09} _{-0.10}	8.62	0.95	14.24	0.5	-0.1	21.93 ± 0.01	1.2
131	J142509.2+353527	14:25:09.23	35:35:27.5	0.8''	71.0 ^{+10.1} _{-9.0}	9.2 ^{+4.6} _{-3.4}	61.8 ^{+9.4} _{-8.3}	TSH	0.74 ^{+0.09} _{-0.11}	5.53	0.27	11.24	-0.3	-0.0	20.85 ± 0.01	1.0
132	J142505.1+354054	14:25:05.16	35:40:54.9	0.8''	205.0 ^{+16.4} _{-15.3}	131.2 ^{+13.2} _{-12.1}	73.8 ^{+10.4} _{-9.3}	TSH	-0.27 ^{+0.08} _{-0.07}	17.72	4.27	15.01	-0.5	0.6	22.59 ± 0.04	1.0
133	J142504.4+353514	14:25:04.47	35:35:14.6	1.5''	39.9 ^{+8.6} _{-7.5}	26.7 ^{+6.8} _{-5.6}	13.2 ^{+6.1} _{-4.9}	TS	-0.33 ^{+0.21} _{-0.19}	3.17	0.80	2.45	0.3	-0.7	23.16 ± 0.06	1.0
134	J142503.9+353345	14:25:03.90	35:33:45.7	1.5''	42.4 ^{+8.7} _{-7.6}	13.5 ^{+5.5} _{-4.3}	28.9 ^{+7.3} _{-6.2}	TSH	0.37 ^{+0.17} _{-0.19}	4.40	0.52	7.04	-0.9	-0.2	20.29 ± 0.00	1.0
135	J142503.1+353421	14:25:03.16	35:34:21.2	1.2''	60.3 ^{+10.1} _{-9.0}	13.5 ^{+5.8} _{-4.7}	46.8 ^{+8.8} _{-7.7}	TSH	0.56 ^{+0.13} _{-0.15}	4.85	0.41	8.82	1.1	0.5	>25.7	...

Table 1—Continued

ID	CXOLALA1	RA(J2000)	Dec(J2000)	Err	Tot. Cts.	Soft Cts.	Hard Cts.	det	HR	S _{0.5–10}	S _{0.5–2}	S _{2–10}	Δα(")	Δδ(")	R	FWHM(")
136	J142502.9+353512	14:25:02.94	35:35:12.8	1.0''	112.1 ^{+12.7} _{-11.6}	69.9 ^{+10.0} _{-8.9}	42.2 ^{+8.5} _{-7.3}	TSH	-0.24 ^{+0.11} _{-0.11}	9.08	2.12	8.00	-0.6	-0.2	25.11 ± 0.31	1.1
137	J142501.2+353622	14:25:01.20	35:36:22.0	1.2''	93.5 ^{+11.9} _{-10.8}	66.5 ^{+9.9} _{-8.8}	27.1 ^{+7.4} _{-6.3}	TSH	-0.42 ^{+0.12} _{-0.11}	7.82	2.08	5.31	0.5	0.0	23.12 ± 0.05	1.0
138	J142457.3+353627	14:24:57.33	35:36:27.5	1.2''	93.5 ^{+12.1} _{-11.0}	45.3 ^{+8.6} _{-7.5}	48.1 ^{+9.2} _{-8.1}	TSH	0.04 ^{+0.12} _{-0.13}	7.63	1.39	9.24	0.5	0.2	>25.7	...
139	J142454.8+353431	14:24:54.80	35:34:31.9	0.9''	250.3 ^{+18.3} _{-17.2}	157.6 ^{+14.4} _{-13.3}	92.7 ^{+12.0} _{-10.9}	TSH	-0.25 ^{+0.07} _{-0.07}	22.73	5.36	19.83	0.2	-0.7	20.50 ± 0.01	1.1
140	J142616.9+353729	14:26:16.94	35:37:29.4	1.9''	71.1 ^{+10.9} _{-9.8}	23.4 ^{+6.9} _{-5.7}	47.6 ^{+9.0} _{-7.9}	TSH	0.35 ^{+0.13} _{-0.15}	5.91	0.73	9.29	0.9	0.7	23.11 ± 0.06	1.5
141	J142613.9+353445	14:26:13.97	35:34:45.5	1.6''	35.4 ^{+8.6} _{-7.5}	26.6 ^{+6.9} _{-5.7}	8.8 ^{+5.9} _{-4.8}	TS	-0.50 ^{+0.24} _{-0.21}	2.81	0.79	1.64	>25.7	...
142	J142601.7+354037	14:26:01.72	35:40:37.5	1.3''	19.4 ^{+6.6} _{-5.4}	12.4 ^{+5.1} _{-3.9}	7.0 ^{+4.9} _{-3.7}	TS	-0.28 ^{+0.32} _{-0.30}	1.85	0.44	1.56	0.2	-0.8	23.55 ± 0.09	1.0
143	J142601.7+352802	14:26:01.71	35:28:02.8	2.7''	17.8 ^{+7.8} _{-6.7}	7.4 ^{+5.2} _{-4.0}	10.4 ^{+6.5} _{-5.3}	T	0.17 ^{+0.37} _{-0.42}	2.14	0.33	2.93	0.8	0.3	23.11 ± 0.06	1.8
144	J142530.9+352756	14:25:30.95	35:27:56.8	2.4''	17.7 ^{+6.3} _{-5.1}	14.6 ^{+5.3} _{-4.2}	3.1 ^{+4.1} _{-2.9}	TS	-0.64 ^{+0.33} _{-0.26}	5.16	1.58	2.15	0.6	-0.9	20.75 ± 0.01	1.3
145	J142527.5+352656	14:25:27.53	35:26:56.2	3.1''	21.8 ^{+6.8} _{-5.6}	18.3 ^{+5.8} _{-4.7}	3.5 ^{+4.3} _{-3.1}	TS	-0.67 ^{+0.29} _{-0.22}	6.05	1.90	2.29	-0.3	0.9	17.44 ± 0.00	1.1
146	J142524.4+352542	14:25:24.40	35:25:42.1	2.5''	61.3 ^{+9.7} _{-8.6}	39.2 ^{+7.8} _{-6.6}	22.0 ^{+6.6} _{-5.4}	TS	-0.27 ^{+0.15} _{-0.14}	18.44	4.42	15.73	-0.7	-0.4	21.50 ± 0.01	1.0
147	J142519.7+354432	14:25:19.79	35:44:32.2	2.1''	70.7 ^{+11.1} _{-10.0}	50.7 ^{+9.0} _{-7.9}	20.0 ^{+7.3} _{-6.2}	TS	-0.43 ^{+0.15} _{-0.14}	7.44	2.01	4.98	-0.5	0.4	21.89 ± 0.02	1.0
148	J142517.7+353754	14:25:17.71	35:37:54.3	1.1''	11.4 ^{+4.9} _{-3.7}	1.2 ^{+2.8} _{-1.2}	10.2 ^{+4.6} _{-3.4}	T	0.79 ^{+0.18} _{-0.37}	1.40	0.05	2.92	0.7	-0.6	24.48 ± 0.17	1.3
149	J142516.0+354325	14:25:16.02	35:43:25.8	2.3''	17.6 ^{+8.2} _{-7.1}	21.1 ^{+6.7} _{-5.5}	0.0 ^{+5.6} _{-0.0}	TS	-1.00 ^{+0.38} _{-0.00}	1.43	0.64	< 1.07	>25.7	...
150	J142505.2+353729	14:25:05.25	35:37:29.5	1.6''	21.6 ^{+6.9} _{-5.7}	19.3 ^{+6.1} _{-4.9}	2.3 ^{+4.1} _{-2.3}	TS	-0.78 ^{+0.29} _{-0.17}	1.78	0.60	0.45	0.2	-0.2	>25.7	...
151	J142503.5+353859	14:25:03.57	35:38:59.2	1.7''	37.7 ^{+8.3} _{-7.2}	22.6 ^{+6.3} _{-5.1}	15.0 ^{+6.2} _{-5.0}	TS	-0.20 ^{+0.21} _{-0.20}	3.09	0.70	2.90	-0.6	-0.2	20.26 ± 0.01	1.2
152	J142501.5+354000	14:25:01.58	35:40:00.3	1.9''	52.2 ^{+9.6} _{-8.5}	35.0 ^{+7.6} _{-6.5}	17.2 ^{+6.6} _{-5.4}	TS	-0.34 ^{+0.18} _{-0.16}	4.26	1.07	3.30	1.0	-1.6	23.70 ± 0.08	1.0
153	J142501.2+353057	14:25:01.28	35:30:57.4	2.2''	36.6 ^{+9.1} _{-8.0}	15.1 ^{+6.1} _{-4.9}	21.5 ^{+7.4} _{-6.3}	TSH	0.18 ^{+0.22} _{-0.24}	3.54	0.55	4.90	-1.7	0.1	23.91 ± 0.08	1.0
154	J142459.2+353751	14:24:59.24	35:37:51.4	1.8''	35.4 ^{+8.5} _{-7.3}	21.5 ^{+6.6} _{-5.4}	13.8 ^{+6.1} _{-4.9}	TS	-0.21 ^{+0.23} _{-0.22}	2.89	0.66	2.66	-0.6	-0.4	21.61 ± 0.02	1.2
155	J142611.8+353301	14:26:11.85	35:33:01.9	1.7''	20.5 ^{+7.2} _{-6.1}	1.8 ^{+4.0} _{-1.8}	18.7 ^{+6.6} _{-5.4}	T	0.83 ^{+0.15} _{-0.30}	1.64	0.05	3.51	-0.4	0.6	22.63 ± 0.03	1.1
156	J142540.2+354623	14:25:40.21	35:46:23.0	3.8''	24.6 ^{+7.5} _{-6.4}	5.3 ^{+4.3} _{-3.1}	19.2 ^{+6.7} _{-5.5}	T	0.57 ^{+0.21} _{-0.27}	6.70	0.55	12.41	-0.7	1.1	16.33 ± 0.00	1.6
157	J142539.8+354438	14:25:39.87	35:44:38.6	2.4''	26.3 ^{+8.3} _{-7.2}	10.2 ^{+5.6} _{-4.4}	16.1 ^{+6.8} _{-5.6}	T	0.23 ^{+0.27} _{-0.30}	2.55	0.37	3.70	-1.3	0.4	19.91 ± 0.01	1.2
158	J142531.6+352659	14:25:31.60	35:26:59.0	3.5''	29.8 ^{+7.5} _{-6.4}	4.7 ^{+4.1} _{-2.9}	25.1 ^{+6.8} _{-5.6}	TH	0.69 ^{+0.16} _{-0.22}	8.74	0.52	17.35	2.1	2.0	24.71 ± 0.15	1.0
159	J142448.4+353227	14:24:48.48	35:32:27.4	2.8''	40.6 ^{+9.8} _{-8.7}	26.4 ^{+7.3} _{-6.2}	14.2 ^{+7.2} _{-6.1}	T	-0.29 ^{+0.24} _{-0.23}	5.80	1.41	4.83	-0.6	1.0	24.00 ± 0.14	1.1
160	J142447.8+353138	14:24:47.80	35:31:38.8	3.3''	22.2 ^{+9.0} _{-7.9}	13.7 ^{+6.1} _{-4.9}	8.5 ^{+7.2} _{-6.1}	T	-0.22 ^{+0.38} _{-0.39}	3.07	0.71	2.81 ^b	...
161	J142528.8+353342	14:25:28.80	35:33:42.0	0.6''	7.7 ^{+4.3} _{-3.1}	5.8 ^{+3.8} _{-2.5}	1.9 ^{+3.1} _{-1.7}	S	-0.50 ^{+0.51} _{-0.36}	0.57	0.16	0.33	0.6	-0.1	19.52 ± 0.00	1.3
162	J142558.2+353144	14:25:58.29	35:31:44.4	1.6''	12.3 ^{+5.9} _{-4.8}	6.0 ^{+4.1} _{-2.9}	6.3 ^{+4.9} _{-3.7}	S	0.04 ^{+0.41} _{-0.45}	0.97	0.18	1.17	0.5	-0.2	25.08 ± 0.26	1.3
163	J142458.1+353919	14:24:58.14	35:39:19.4	2.5''	25.6 ^{+8.2} _{-7.1}	16.9 ^{+6.2} _{-5.0}	8.7 ^{+6.2} _{-5.0}	S	-0.32 ^{+0.31} _{-0.29}	2.58	0.64	2.06	0.8	0.1	25.21 ± 0.27	0.9
164	J142535.9+353102	14:25:35.96	35:31:02.8	1.1''	14.4 ^{+5.7} _{-4.5}	0.0 ^{+2.4} _{-0.0}	15.3 ^{+5.6} _{-4.4}	H	1.00 ^{+0.00} _{-0.25}	1.11	< 0.07	2.78	-0.2	-0.4	23.53 ± 0.08	1.5
165	J142527.4+353257	14:25:27.46	35:32:57.9	0.6''	8.6 ^{+4.5} _{-3.3}	0.0 ^{+1.9} _{-0.0}	9.8 ^{+4.5} _{-3.3}	H	1.00 ^{+0.00} _{-0.32}	0.66	< 0.06	1.76	0.8	-0.6	24.80 ± 0.31	1.3
166	J142545.4+352711	14:25:45.44	35:27:11.8	2.5''	19.8 ^{+7.2} _{-6.0}	1.2 ^{+3.8} _{-1.2}	18.6 ^{+6.6} _{-5.4}	H	0.89 ^{+0.10} _{-0.30}	3.05	0.07	6.77	-1.9	-0.0	23.48 ± 0.07	1.2
167	J142523.4+353512	14:25:23.49	35:35:12.4	0.7''	6.5 ^{+4.3} _{-3.1}	0.0 ^{+2.4} _{-0.0}	6.6 ^{+4.1} _{-2.9}	H	1.00 ^{+0.00} _{-0.55}	0.50	< 0.07	1.17	0.1	-0.4	20.80 ± 0.01	1.3
168	J142621.6+353931	14:26:21.63	35:39:31.1	3.2''	23.2 ^{+8.2} _{-7.0}	1.6 ^{+4.1} _{-1.6}	21.7 ^{+7.5} _{-6.4}	H	0.87 ^{+0.12} _{-0.28}	2.71	0.07	5.96	1.4	-2.1	>25.7	...

^aSource No. 22 is overlapped by bleeding of charge in the NDWFS *R* image we used in this paper. Source position and *R* band magnitude were measured from an older version of the NDWFS *R* image.^bSource No. 37 and 160 are overlapped by bleeding of charge in both the NDWFS *R* and the older NDWFS *R* images